Adaption of the PC-Ellipsometry for the Condensed Krypton Calibration Source Setup, Converted for the Operation at the KATRIN-Experiment

Simon-Nis Peters
s_pete17@wwu.de

Abschlussarbeit
im Fachbereich Physik
der WWU Münster
December 10, 2015

Referent: Prof. Dr. C. Weinheimer
Korreferent: Apl. Prof. Dr. A. Khoukaz

Hol mal die Zange.
—Wes

Contents

1 Introduction

When Lise Meitner and Otto Hahn first measured the energy spectrum of the β-decay in 1911 they saw multiple lines on a defuse background, this indicated a continuous energy spectrum. Since in that time it was thought, the β-decay would be a two body problem (the atom emitting an electron), they where puzzled. A continuous spectrum would violate the conservation of energy. In 1930 Wolfgang Pauli, desperate to safe the laws of energy conservation, hypothesized a third neutral particle would participate in the β-decay, the neutrino[1]. Four years later Enrico Fermi developed a model for the β-decay, this model described the neutrino as a massless neutral particle. It took another 22 years to actually detect the neutrino in the Cowan–Reines neutrino experiment. Inside the standard model of particle physics the neutrino was first expected to be massless. [Mur02] Today we know that neutrinos come in three flavours, the electron- (ν_e), muon- (ν_μ) and tau-neutrino (ν_τ). These flavours can oscillate into one another, as proven by many experiments and rewarded with the Nobel price in physics in 2015 to Takaaki Kajita[2] and Arthur B. McDonald[3]. This neutrino flavour oscillation proves, that the neutrino can not be massless. By now many experiments have investigated and found upper limits for the neutrino mass.
Measuring the neutrino mass or improving the upper limit would be of help in understanding the origin of the universe.

[1] The original name Pauli gave to the particle was Neutron, but James Chadwick discovered in 1932 the particle we today call the Neutron. The name Neutrino was given by Enrico Fermi, freely translated neutrino means “the little neutral one”
[2] Kamikande-collaboration
[3] SNO-collaboration

1.1 KATRIN

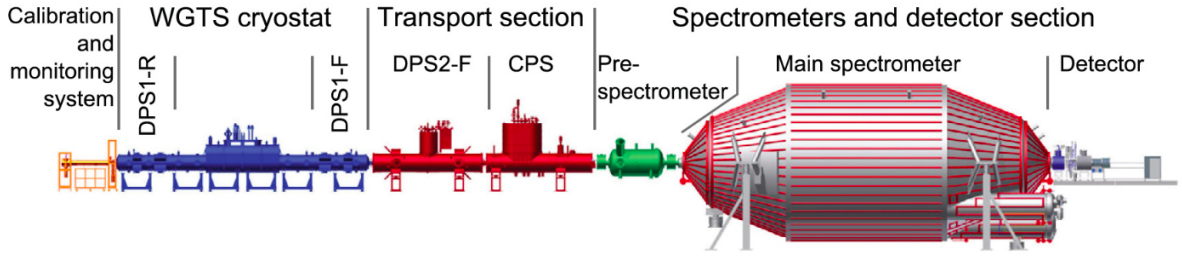

Figure 1.1 – Schematic overview of the Katrin-experiment [al.12].

The **Ka**rlsruhe **Tri**tium **N**eutrino Experiment, or short KATRIN, is an experiment that seeks a better understanding of the tritium β-decay. One of the main components is a large spectrometer, that uses the MAC-E filter[4] principle, to measure the energy spectrum of the tritium β-decay.

A MAC-E-filter consists of two solenoids, creating a strong magnetic field that guides the electrons adiabatically, along the magnetic field lines, in a cyclotron motion through the spectrometer (figure 1.2). A negative voltage is applied to the spectrometer vessel, repelling incoming electrons. Towards the analysing plane the magnetic field strength drops by several orders of magnitude. The analysing plane is characterized by the highest electric field strength and the lowest magnetic field. The slow drop in field strength results in the magnetic gradient force transforming most of the cyclotron energy into longitudinal motion, the magnetic momentum stays constant:

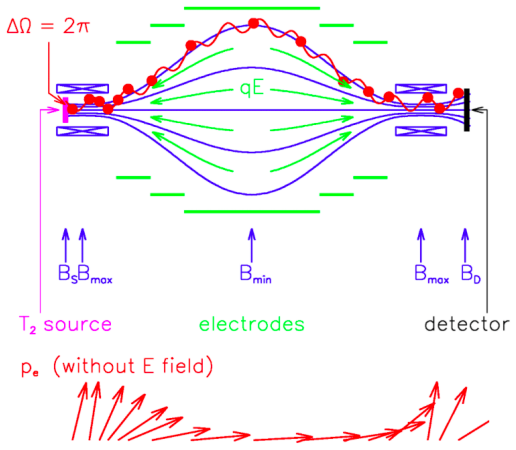

Figure 1.2 – MAC-E-filter [KIT]

$$\mu = \frac{E_\perp}{B} = \text{const.}$$

Electrons with enough energy are able to pass the analysing plane, lower energetic

[4] magnetic adiabatic collimation with an electrostatic filter

electrons are reflected. By varying the applied voltage an integrated spectrum is taken. The resolution ΔE of the spectrometer is influenced by the ratio of the minimal to the maximal magnetic field:

$$\frac{\Delta E}{E} = \frac{B_{\min}}{B_{\max}} \quad . \tag{1.1.1}$$

The high acceptance angle for incoming electrons with a polar angle smaller than 51° results in high luminosity, electrons with a bigger polar angle are reflected at the pinch magnet. With KATRIN it is expected to gain a model independent upper limit of the anti-electron-neutrino mass $m_{\bar{\nu}_e}$. With an accuracy for the upper limit of 200 meV (90 % C.L.) KATRIN will surpass the accuracy of former direct neutrino mass experiments, like Troisk and Mainz, by one order of magnitude [AP92], [Lob03]. If the neutrino mass is above 0.35 eV, KATRIN will be able to measure the neutrino mass with a confidence level of 5σ.

Figure 1.1 shows a schematic overview of the KATRIN-experiment. It is divided into 3 major parts.

The source is a **w**indowless **g**asious **t**ritium **s**ource (WGTS), located on the left (blue). It contains a 10 m long pipe with a diameter of 90 mm at 30 K. Inside this pipe tritium is circulated with a pressure of $3.35 \cdot 10^{-3}$ mbar $- 4 \cdot 10^{-5}$ mbar. The WGTS will have an activity of 10^{11} Bq. Further details can be obtained in [col04].

The WGTS is followed by the transport section which consists of a **d**ifferential **p**umping **s**ection (DPS2) and a **c**ryogenic **p**umping **s**ection (CPS). This section protects the main spectrometer from contamination with tritium, reducing the background. While guiding the electrons magnetically into the the main spectrometer, the flux of tritium atoms is reduced by a factor of 10^{14}, from 2 $\frac{\text{mbar}\cdot\text{l}}{\text{s}}$ at the entrance of the DPS2-F to 10^{-14} $\frac{\text{mbar}\cdot\text{l}}{\text{s}}$ at the main spectrometer [col04], [Stu07].

The spectrometer section consists of the pre and main spectrometer[5]. The pre spectrometer is 3.3 m long and 1.7 m in diameter. Reducing the electron flux from 10^{10} to 10^3 electrons per second, it serves a high pass filer to the main spectrometer. The magnetic field in the pre spectrometer is generated by two solenoids, each generating a 4.5 T strong magnetic field, which drops to 20 mT in the analysing plane. This results in an energy resolution of 100 eV for 18.6 keV electrons, which is good enough for the use as a pre filter. [Thu07]

[5] both use the MAC-E-filter principle.

The second solenoid of the pre spectrometer is also used to generate the magnetic field of the main spectrometer, which is a 24 m long tank that has a diameter of 10 m. These dimensions are a consequence of equation 1.1.1, a bigger vessel results in a higher resolution, while at the same time allowing for a large acceptance. The function of the second solenoid is covered by the magnets of the detector, which is placed at the end of the main spectrometer. The magnetic field falls to 0.3 mT, in the analysing plane, resulting in a much higher energy resolution of 0.93 eV for 18.6 keV electrons. This low magnetic field makes it necessary to compensate the magnetic field of the earth[6] [Thu07]. Additional to the magnetic shielding, a system of wire electrodes are mounted inside the spectrometer vessel to reduce the background. By putting them on a slightly more negative potential than the vessel, electrons generated from radioactive decays or cosmic muons inside the spectrometer are guided back to the spectrometer wall. The wire electrode system is also used for fine tuning the retardation voltage [Val09]. Since minor changes in the retardation voltage σ will result in a negative systematic shift of the neutrino mass [Rob88]

$$\Delta m_\nu^2 = -2\sigma^2 \quad , \tag{1.1.2}$$

it is important to know the retardation voltage with high accuracy. A system of calibration mechanism will be used to monitor the long term stability in the retardation voltage.

1.1.1 The condensed Krypton calibration source

The condensed Krypton calibration source **(CKrS)**, seen in figure 1.4a, will among other systems be used to monitor the stability of the retardation voltage at the KATRIN-experiment. In order to achieve the targeted sensitivity for the neutrino mass of $m_{\bar{\nu}_e} < 0.2\,\text{eV}$ the long term drift of the retardation voltage with the width of σ must be smaller than 60 mV. The analysing plane will be on a potential near 18.6 keV resulting in required resolution of $\frac{0.06\,\text{V}}{18576\,\text{V}} \simeq 3\,\text{ppm}$ for the voltage stability. To calibrate the retarding potential of the KATRIN-main-spectrometer, the CKrS uses a thin ^{83m}Kr film, that is

[6] air coils surround the main spectrometer, these aircoils also can be used for fine adjustments of the magnetic flux tube.

adsorbed on a HOPG[7], to generate electrons with well defined properties[8].

Conversion electrons of ^{83m}Kr

^{83m}Kr is an exited isomer of krypton, generated by an electron capture from the mother isotope ^{84}Rb. It has a half-life of $t_{1/2} = 1.83\,\text{h}$ and an excitation energy of 41.55 keV. The decay from $I = \frac{1}{2}^-$ to $I = \frac{7}{2}^+$ via internal conversion is a factor[9] $\alpha = 2000$ more probable than the emission of a γ-quantum. The energy of this decay is 32.151 keV, the emitted electron has an energy of $E_{K-conversion} = 17.824\,\text{keV}$ with a linewidth of $\Delta E_{conversion} = 2.83\,\text{eV}$ (FWHM)[10]. The short half-life and the fact, that $E_{K-conversion}$ is close to the endpoint of the tritium β-decay make ^{83m}Kr a good choice for calibrating the main spectrometer. The state $I = \frac{7}{2}^+$ has a half-life of $t_{1/2} = 154.4\,\text{ns}$ and decays into $I = \frac{9}{2}^+$, which minimizes the risk of long-term contamination of the spectrometer.

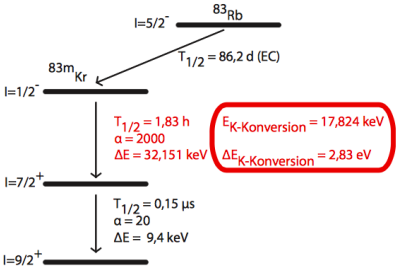

Figure 1.3 – Decay of ^{83}Rb to ^{83}Kr [Weg10]

Requirements to the CKrS

The CKrS has to fulfil many requirements, such as a stable position of the spectral line (which should be close to the endpoint of the β-decay of tritium) and a high count rate. Next to calibrating the retardation voltage, the CKrS will be used to determine the transmission function of the main-spectrometer in-between measurement phases. For this purpose the count rate needs to be within a range of $2 - 3\,\text{kHz}$, this rate can be achieved by the CKrS, as presented in [Smo08]. In order to scan the entire flux tube the CKrS will be mounted movable as seen in figure 1.4b. The exact set up is explained in [Bau13]. The stability of the spectral linewidth will be achieved by the cleanness

[7] highly ordered pyrolitic graphite

[8] ^{83m}Kr is used because the conversion electrons of its K-shell have a energy of $E_{K-conversion} = 17.824\,\text{keV}$ which is close to the endpoint of the tritium β-decay at $E = 18.6\,\text{keV}$

[9] internal conversion coefficient $\alpha = \frac{e}{\gamma}$, where e is is the measured rate of conversion electrons and γ the rate for γ-ray emissions.

[10] Full width half maximum

and sub-mono layer thickness of the film. The properties of the film will be monitored using laser ellipsometry [Ost09], [Bau13]. Even though the light used for measuring has a wavelength of several hundred nanometers, ellipsometry has a resolution in the sub-nanometer range. This high resolution is needed, since only very thin films result in a sharp spectral linewidth. If the film is to thick, electrons from lower layers could loose energy due to scattering, flattening the peak and resulting in a higher uncertainty in the retardation voltage. For the better reproducibility of applied films, the HOPG is cleaned by a combination of Laser-ablation and heating [Gre13]. Additional, an automatic gas system, as described in [Sch11], is used to generate reproducible film thicknesses. To minimize the risk of contamination of the spectrometer with ^{83}Rb, the production of ^{83m}Kr will be in a separated volume [Bau13].

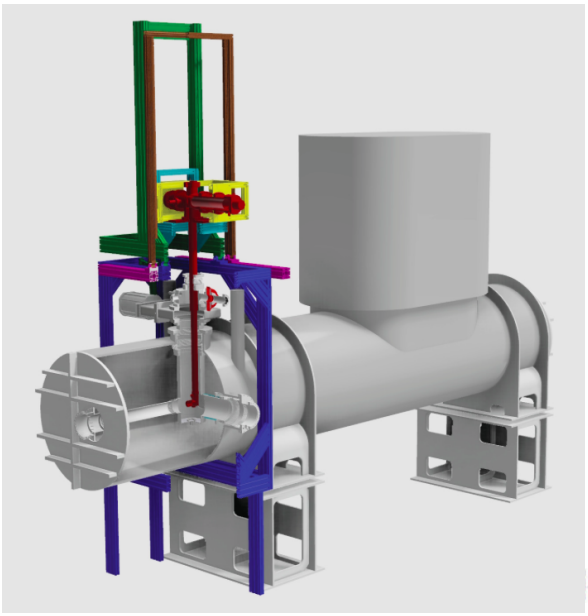

(a) CKrS inside the CPS, the CkrS will be mounted in a way that it can scan the entire flux tube.

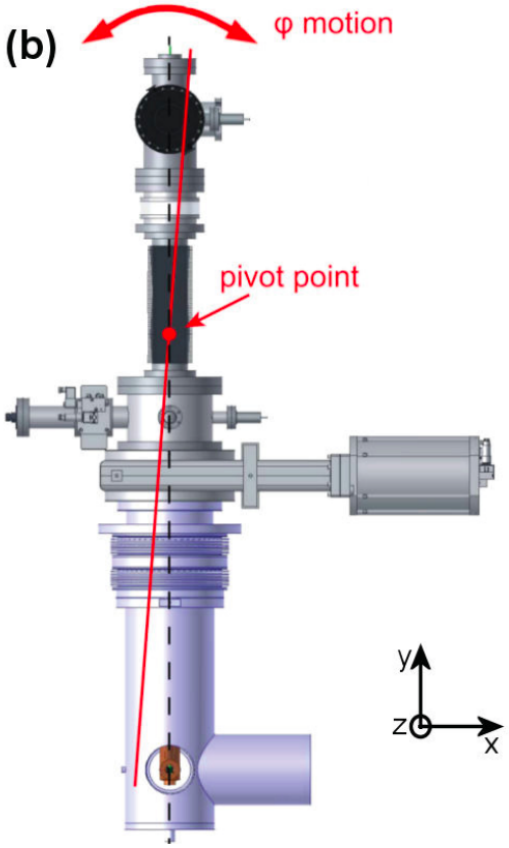

(b) CKrS front view, in order to scan the entire flux tube the CKrS can be lifted in y-direction and tilted around the pivot point.

Figure 1.4 – Condensed Krypton Calibration Source, CAD-drawing of the set up for the CPS.

2 Theory of ellipsometry

Ellipsometry utilizes the fact that light can change its state of polarization upon the interaction with matter. By analysing this change in a well defined set up, properties of thin films can be analysed.

2.1 Polarization of Light

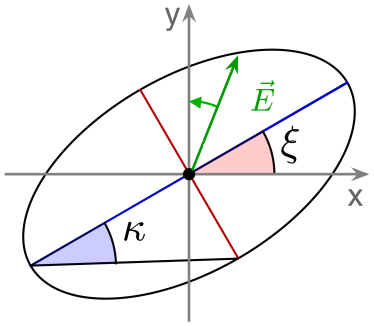

(a) The shape of the ellipse is given by the ellipticity angle κ, for a positive κ, the E-field vector rotates counter clockwise, for negative clockwise. The tilt of the ellipse is given by tilt angle ξ.

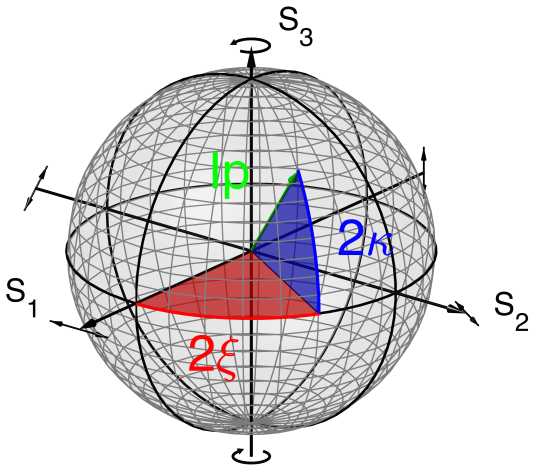

(b) The three Stokes vectors represent any type of polarisation given in the polarisation ellipse. The azimuthal angle $2\,\xi$ gives the tilt of the ellipse, while the polar angle $2\,\kappa$ gives the shape.

Figure 2.1 – Representations of polarisations, polarisation ellipse **(a)** and Poincaresphere **(b)**

Light can be described as an planar electromagnetic wave (EMW), characterized by its wave vector $\vec{k}$, the electric field $\vec{E}$, the magnetic field $\vec{H}$, the electric displacement field $\vec{D}$ and the magnetic flux density $\vec{B}$. Since $\vec{E}$ has the biggest impact on the

force applied to electrons, in the interaction of light with matter, it is defined as the direction of polarization. All other field vectors can be derived from it, using the Maxwell equations [Azz77]. Every electromagnetic wave can be written as a superposition of two orthogonal polarized waves, propagating in z-direction, it can be written as:

$$\vec{E}(z,t) = \exp\left[i(kz - \omega t)\right] \left(\tilde{E}_x \hat{e}_x + \tilde{E}_y \hat{e}_y\right), \tag{2.1.1}$$

where

k	$= \frac{2\pi}{\lambda}$	describes the wave vector,
ω	$= 2\pi f$	the angular frequency,
$\tilde{E}_j$	$= \varepsilon_j \cdot \exp[i\,\delta_j]$	the complex amplitude for $j = x, y$, where δ is the phase and
$\hat{e}_x$,$\hat{e}_y$		are the basis vectors

As only the intensity of light can be measured, the imaginary part is neglected and just the real part of the electric field is of interest:

$$\vec{\varepsilon}(z,t) = \varepsilon_x \hat{e}_x \cos(kz - \omega t) + \varepsilon_y \hat{e}_y \cos(kz - \omega t + \delta). \tag{2.1.2}$$

$\delta = \delta_x - \delta_y$ is the phase difference, which is needed to describe the polarisation state [Jac02]. A way to represent the polarisation, is in form of an ellipse figure 2.1a. Here the orientation of the ellipse is given by the angle $\xi := \{0, \pi\}$ and the shape by the ellipticity angle $\kappa := \{-\frac{\pi}{4}, \frac{\pi}{4}\}$. The ellipse describes the movement of the electric field vector over time. Every shape of the ellipse corresponds to a relative phase difference δ. The three major types of polarization are, linear, circular and elliptical polarization.

linear	$\delta = 0, \pm\pi, \pm 2\pi, \cdots$
	$\kappa = 0$
	$\xi = \{0, \pi\}$
circular	$\delta = \pm\frac{\pi}{2}, \pm\frac{3\pi}{2}, \cdots$
	$\kappa = \frac{\pi}{4}, \frac{\pi}{4}$
	ξ is not relevant
elliptical	in all other cases, the light is elliptically polarized.

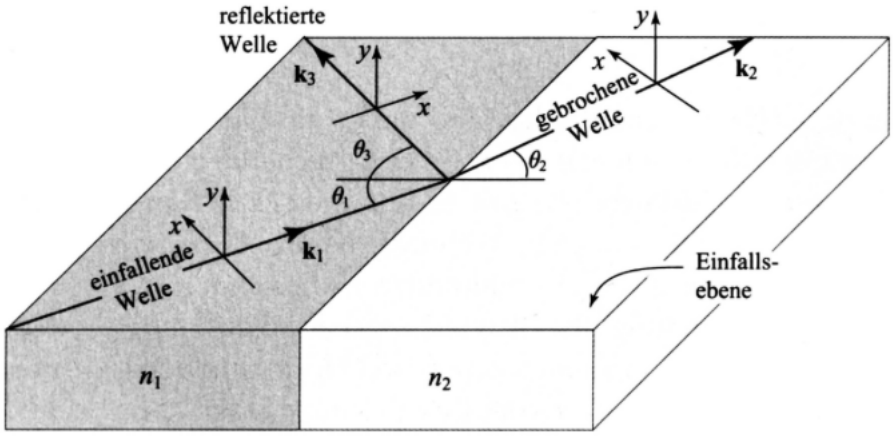

Figure 2.2 – Reflection of light on the interface between two dielectric materials with refractive indices n_1 and n_2. [Sal08]

2.1.1 Reflection/Refraction

If a beam of monochromatic light (index 1) hits the boundary between two isotropic materials the beam is split into a reflected (index 3) and refracted beam (index 2), shown figure 2.2. The angle θ of the incoming beam towards the surface normal is equal to the angle θ_3 of the reflected ray with the same normal. The refracted beam at angle θ_2 can be calculated using Snell's law of refraction:

$$n_1 \sin\theta_1 = n_2 \sin\theta_2 \quad , \tag{2.1.3}$$

where n_1 and n_2 are the refractive indices of the isotropic materials. All rays lay in the so called "plane of incidence". The relation between transmission coefficient t and reflection coefficient r depends on the polarization and angle of incidence. As mentioned in equation 2.1.2 light can be described as a superposition of two orthogonal electromagnetic waves. If one of those waves is chosen in way, that its polarization is in the plane of incidence, it is called p-polarized (parallel-polarized). Since the other wave is orthogonal to the first and $\vec{k_1}$, it is perpendicular to the plane of incidence, thus called s-polarized[1]. The complex transmission- and reflection- indices are described by the Fresnel equations, using the nomenclature of figure 2.2 they can be written as:

[1] "Senkrecht" German for perpendicular

$$r_\mathrm{p} = r_\mathrm{x} = \frac{n_2 \cos\theta_1 - n_1 \cos\theta_2}{n_2 \cos\theta_1 + n_1 \cos\theta_2} \tag{2.1.4}$$

$$r_\mathrm{s} = r_\mathrm{y} = \frac{n_1 \cos\theta_1 - n_2 \cos\theta_2}{n_1 \cos\theta_1 + n_2 \cos\theta_2} \tag{2.1.5}$$

$$t_\mathrm{p} = t_\mathrm{x} = (1 + r_\mathrm{p}) \frac{\cos\theta_1}{\cos\theta_2} \tag{2.1.6}$$

$$t_\mathrm{s} = t_\mathrm{y} = 1 + r_\mathrm{s}. \tag{2.1.7}$$

2.2 Mathematics of polarization

"Two algebraic systems have been developed for the solution of polarization problems in optics, the Jones formalism, and the Mueller Stokes formalism. The Jones formalism is a natural consequence of the mathematical phase and amplitude description of light. The Mueller-Stokes formalism comes from an experimental consideration of the intensity measurements of light." [Gol10]

2.2.1 Mueller-Stokes formalism

In Mueller calculus the state of polarization is given by four dimensional Stokes vectors $\vec{S}$:

$$\vec{S} = \begin{pmatrix} S_0 \\ S_1 \\ S_2 \\ S_3 \end{pmatrix}. \tag{2.2.1}$$

Where S_0 gives the total intensity of the beam, S_1 and S_2 give the amount of linear polarized light and S_3 the proportion of circular polarized light. A few examples of polarization states in form of a Stokes vector are given in table 2.1.

Example polarization types in Stokes vectors

	linear 0° (horizontal)	linear 90° (vertical)	linear 45°	linear −45°	right hand circular	left hand circular	unpolarized
$\begin{pmatrix} S_0 \\ S_1 \\ S_2 \\ S_3 \end{pmatrix}$	$\begin{pmatrix} 1 \\ 1 \\ 0 \\ 0 \end{pmatrix}$	$\begin{pmatrix} 1 \\ -1 \\ 0 \\ 0 \end{pmatrix}$	$\begin{pmatrix} 1 \\ 0 \\ 1 \\ 0 \end{pmatrix}$	$\begin{pmatrix} 1 \\ 0 \\ -1 \\ 0 \end{pmatrix}$	$\begin{pmatrix} 1 \\ 0 \\ 0 \\ 1 \end{pmatrix}$	$\begin{pmatrix} 1 \\ 0 \\ 0 \\ -1 \end{pmatrix}$	$\begin{pmatrix} 1 \\ 0 \\ 0 \\ 0 \end{pmatrix}$

Table 2.1 – Examples for linear, circular and elliptical light in the Mueller-Stokes formalism

Optical instruments like polarisers or quaterwave plates can be described via 4×4 Mueller matrices. The transformation of an incoming beam $\vec{S_i}$, by an optical instrument with Mueller matrix M is described by matrix multiplication

$$\vec{S_o} = \mathrm{M} \cdot \vec{S_i} \quad , \tag{2.2.2}$$

where $\vec{S_o}$ is the outgoing beam.

Poincare sphere

The Stokes parameters can be displayed in form of a "Poincaresphere" (figure 2.1b). It uses the angles given in (figure 2.1a) to represent all types of polarization on a unit sphere. In spherical coordinates each position on the sphere represents a pair of κ and ξ, which are related to the stokes parameters (S_0, S_1, S_2, S_3) in Cartesian coordinates via:

$$\begin{aligned} S_0 &= I \\ S_1 &= Ip \cos 2\xi \cos 2\kappa \\ S_2 &= Ip \sin 2\xi \cos 2\kappa \\ S_3 &= Ip \sin 2\kappa, \end{aligned}$$

where

I is the intensity and

$p = \frac{\sqrt{S_1+S_2+S_3}}{S_0}$ is the degree of polarization.

The Stokes parameters can also be normalized to the power carried by the polarized part of the light $P\left(=\sqrt{S_1^2+S_2^2+S_3^2}\right)$ and can than be written as:

$$\vec{S} = \frac{1}{P}\begin{pmatrix} S_0 \\ S_1 \\ S_2 \\ S_3 \end{pmatrix}. \tag{2.2.3}$$

Any given polarization can now be displayed on the surface of the sphere with radius r. The distance between two points on that surface D gives the overlap of polarization states:

$$D = \vartheta r \tag{2.2.4}$$

where ϑ is the angle between two stokes vectors in radians

$$\cos\vartheta = \frac{\vec{S'}_1 \cdot \vec{S'}_2}{|\vec{S'}_1|\,|\vec{S'}_2|} \tag{2.2.5}$$

here $\vec{S'}$ just describes the polarisation, neglecting S_0

$$\vec{S'} = \frac{1}{P}\begin{pmatrix} S_1 \\ S_2 \\ S_3 \end{pmatrix} \tag{2.2.6}$$

for two normed stokes vectors ($|\vec{S'_i}| = 1$) with $r = 1$ equation 2.2.4 can be written as

$$D = \arccos\left(\vec{S'_1} \cdot \vec{S'_2}\right) \quad . \tag{2.2.7}$$

A value closer to 0 indicates a strong overlap, while a value closer to π indicates a low overlap.

2.2.2 Jones formalism

Other than the Mueller calculus, the Jones formalism only describes fully polarized light. Here a beam is described via a two dimensional vector $\vec{J}$. Optical instruments such as polarisers, quaterwave plates or reflective surfaces are specified by 2×2 Jones matrices. The rays in figure 2.2 can now be written as:

$$\vec{J}_1 = \begin{bmatrix} \tilde{E}_{\mathrm{x},1} \\ \tilde{E}_{\mathrm{y},1} \end{bmatrix} \qquad \vec{J}_2 = \begin{bmatrix} \tilde{E}_{\mathrm{x},2} \\ \tilde{E}_{\mathrm{y},2} \end{bmatrix} \qquad \vec{J}_3 = \begin{bmatrix} \tilde{E}_{\mathrm{x},3} \\ \tilde{E}_{\mathrm{y},3} \end{bmatrix} \tag{2.2.8}$$

Their amplitudes are are linked via the Jones matrices for refraction $\mathbf{t}$

$$\vec{J}_2 = \mathbf{t}\vec{J}_1 = \begin{bmatrix} t_{\mathrm{x}} & 0 \\ 0 & t_{\mathrm{y}} \end{bmatrix} \cdot \vec{J}_1 = \begin{bmatrix} t_{\mathrm{x}}\tilde{E}_{\mathrm{x},1} \\ t_{\mathrm{y}}\tilde{E}_{\mathrm{y},1} \end{bmatrix} \tag{2.2.9}$$

and reflection $\mathbf{r}$

$$\vec{J}_3 = \mathbf{t}\vec{J}_1 = \begin{bmatrix} r_{\mathrm{x}} & 0 \\ 0 & r_{\mathrm{y}} \end{bmatrix} \cdot \vec{J}_1 = \begin{bmatrix} r_{\mathrm{x}}\tilde{E}_{\mathrm{x},1} \\ r_{\mathrm{y}}\tilde{E}_{\mathrm{y},1} \end{bmatrix} \quad . \tag{2.2.10}$$

$\cos\theta_2$ can be calculated using Snell's law:

$$\begin{aligned} \cos\theta_2 &= \sqrt{1 - \sin^2\theta_2} \\ &= \sqrt{1 - \frac{n_1}{n_2}\sin^2\theta_1} \quad . \end{aligned} \tag{2.2.11}$$

Since $\cos\theta_2$ can be negative the Fresnel coefficients can be written as complex functions:

$$r_{\mathrm{p}} = |r_{\mathrm{p}}| \cdot e^{i\delta_{\mathrm{p}}} \qquad r_{\mathrm{s}} = |r_{\mathrm{s}}| \cdot e^{i\delta_{\mathrm{s}}} \quad . \tag{2.2.12}$$

<table>
<tr><th colspan="3">p-polarisiert</th></tr>
<tr><td>äußere Reflexion
$n_1 < n_2$</td><td> 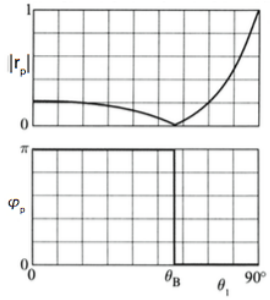 </td><td>$\theta_1 \leq \theta_B$: r_p reell und negativ
• $|r_p|$ fällt von $\frac{n_1-n_2}{n_1+n_2}$ bei $\theta_1 = 0°$ auf 0 beim Brewsterwinkel $\theta_B = \arctan(\frac{n_2}{n_1})$
• $\delta_p = \pi$
$\theta_1 > \theta_B$: r_p reell und positiv
• $|r_p|$ steigt von 0 auf 1 bei 90°
• $\delta_p = 0$</td></tr>
<tr><td>innere Reflexion
$n_1 > n_2$</td><td> 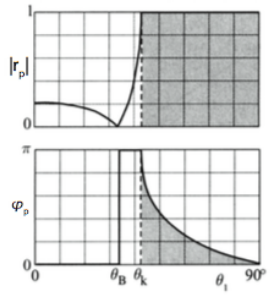 </td><td>$\theta_1 \leq \theta_B$: r_p reell und positiv
• $|r_p|$ fällt von $\frac{n_1-n_2}{n_1+n_2}$ bei $\theta_1 = 0°$ auf 0 bei $\theta_1 = \theta_B$
• δ_p springt bei θ_B von 0 auf π
$\theta_B < \theta_1 \leq \theta_k$: r_p reell und negativ
• $|r_p|$ steigt von 0 auf 1 bei $\theta_1 = \theta_K$
• $\delta_p = \pi$
$\theta_1 > \theta_k$: Innere Totalreflexion, r_p komplex
• $|r_p| = 1$
• δ_p: $\tan\frac{\delta_p}{2} = \frac{-1}{\sin^2\theta_k}\sqrt{\frac{\cos^2\theta_k}{\cos^2\theta_1} - 1}$</td></tr>
<tr><th colspan="3">s-polarisiert</th></tr>
<tr><td>äußere Reflexion
$n_1 < n_2$</td><td> 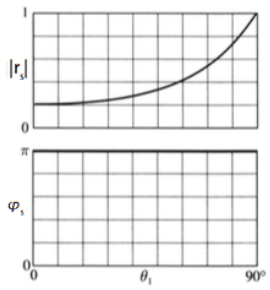 </td><td>r_s ist immer reell und negativ
• $|r_s|$ steigt von $\frac{n_2-n_1}{n_1+n_2}$ bei $\theta_1 = 0°$ kontinuierlich bis auf 1
• $\delta_s = \pi$</td></tr>
<tr><td>innere Reflexion
$n_1 > n_2$</td><td> 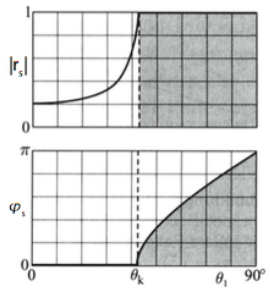 </td><td>$\theta_1 \leq \theta_k$: r_s reell und positiv
• $|r_s|$ steigt von $\frac{n_1-n_2}{n_1+n_2}$ bei $\theta_1 = 0°$ kontinuierlich bis auf 1 bei $\theta_1 = \theta_k = \arcsin\frac{n_2}{n_1}$
• $\delta_s = 0$
$\theta_1 > \theta_k$: Innere Totalreflexion, r_s komplex
• $|r_s| = 1$
• δ_s: $\tan\frac{\delta_s}{2} = \sqrt{\frac{\cos^2\theta_k}{\cos^2\theta_1} - 1}$</td></tr>
</table>

Figure 2.3 – Fresnel coefficients for p- and s- polarized light, for inner and outer reflection. [Sal08]

2.3 Null Ellipsometry

Ellipsometry is a tool to determine optical properties of films or substrates. When light is reflected under an angle $\phi_0 > 0$ from a layer system its state of polarization changes due to the different refractive indices for p- and s- polarized light.

2.3.1 Reflection on a three layer system

The layers in (figure 2.4) can be described via their complex refractive indices N_1, N_2 and N_3. In the following, ambient, film and substrate are treated as isotropic and homogeneous. When a monochromatic, planar EMW with amplitude E_0 hits the surface (**01**) between ambient and film under an angle Φ_0 it is partially reflected and refracted, as described in Section 2.1.1. After propagating the distance $\frac{d}{\cos\Phi_1}$ through the film at angle Φ_1 the light is reflected again at the interface (**12**). Since there is no further layer after the substrate, the refracted part at this boundary is just treated as loss and will not be described any further. The reflected part though, travels the same distance through the film again, and hits the surface (**10**) in opposite direction, where it is reflected and refracted again. This process, in theory, repeats itself infinitely. This allows write the reflected beam as a superposition of infinite reflections, resulting in the reflection coefficient R_j (see equation 2.3.4), where the index j can be substituted with p or s describing the s- and p- polarized part of the ray. The optical path difference Δs of each reflection causes a phase difference between the waves, described by the phase factor $e^{-i2\delta}$. Using Snell's law of refraction Φ_1 is calculated via

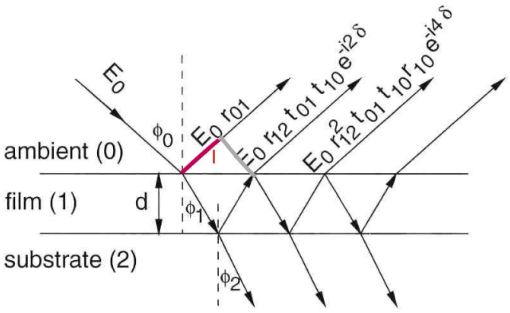

Figure 2.4 – Reflection on a three-layer system. [Weg10]

$$\Phi_1 = \arcsin\left(\frac{N_0}{N_1}\sin\Phi_0\right) \quad , \tag{2.3.1}$$

allowing to write Δs as

$$\begin{aligned}\Delta s &= N_1 \frac{2d}{\cos\Phi_1} - \overbrace{N_0 d \tan\Phi_1 \sin\Phi_0}^{l} \\ &= 2N_1 d \frac{1}{\cos\Phi_1} - N_0 d \frac{N_1}{N_0} \sin\Phi_1 \\ &= 2dN_1 \cos\Phi_1 \quad . \end{aligned} \tag{2.3.2}$$

The phase shift then becomes:

$$\delta = \frac{2\pi}{\lambda} dN_1 \cos\Phi_1 = \frac{2\pi}{\lambda} d\sqrt{N_1^2 - N_0^2 \sin^2\Phi_0} \quad . \tag{2.3.3}$$

R can now be written as the infinite series

$$R_j = r_{01_j} + t_{01_j} t_{10_j} r_{12_j} e^{-i2\delta} + t_{01_j} t_{10} r_{12_j}^2 e^{-i4\delta} + t_{01_j} t_{10} r_{10_j}^2 r_{12_j}^3 e^{-i6\delta} + \cdots \quad , \tag{2.3.4}$$

using

$$\begin{aligned}\sum_{k=0}^{\infty} a_0 q^k &= \lim_{n\to\infty} \sum_{k=0}^{\infty} \\ &= \lim_{n\to\infty} a_0 \frac{1-q^{n+1}}{1-q} \\ &= \frac{a_0}{1-q} \quad , \end{aligned} \tag{2.3.5}$$

it converges to

$$R_j = r_{01_j} + \frac{t_{01_j} t_{10_j} r_{12_j} e^{-i2\delta}}{1 - r_{10_j} r_{12_j} e^{-i2\delta}} \quad . \tag{2.3.6}$$

With

$$r_{01_j} = -r_{10_j} \tag{2.3.7}$$

$$t_{01_j} t_{10_j} = 1 - r_{01_j}^2 \tag{2.3.8}$$

the reflection coefficient can be written as

$$R_j = \frac{r_{01_j} + r_{12_j} e^{-i2\delta}}{1 + r_{10_j} r_{12_j} e^{-i2\delta}} \quad . \tag{2.3.9}$$

The overall transmitted amplitude is given in [Azz77]. The ratio of the complex reflected amplitude is now given by:

$$\rho_\mathrm{s} = \frac{|R_\mathrm{p}|}{|R_\mathrm{s}|} = \tan\Psi e^{i\Delta} \tag{2.3.10}$$

$$\tan\Psi = \frac{R_\mathrm{p}}{R_\mathrm{s}} \tag{2.3.11}$$

$$\Delta = \Delta_\mathrm{p} - \Delta_\mathrm{s} \tag{2.3.12}$$

with Δ_j beeing the complex phase of the reflection amplitude R_j.

2.3.2 Null Ellipsometry in the PCSA-Setup

PA-Ellipsometry

Allowing to determine the complex reflection ρ_s, Null ellipsometry is a powerful tool in thin film analysis. As seen in figure (2.5) a circular polarized laser beam is used as a light source. The light passes through a rotatable polariser at angle P which allows to create linear polarized light with a freely selectable orientation angle ξ and stable amplitude. The polariser is followed by a fixed compensator at angle C (usually a quaterwave plate). This set-up allows to change the ellipticity angle κ from $-\frac{\pi}{4}$ to $\frac{\pi}{4}$ where for every angle of κ there is a fixed angle ξ. Allowing to create all shapes of elliptical polarized light, but just at fixed

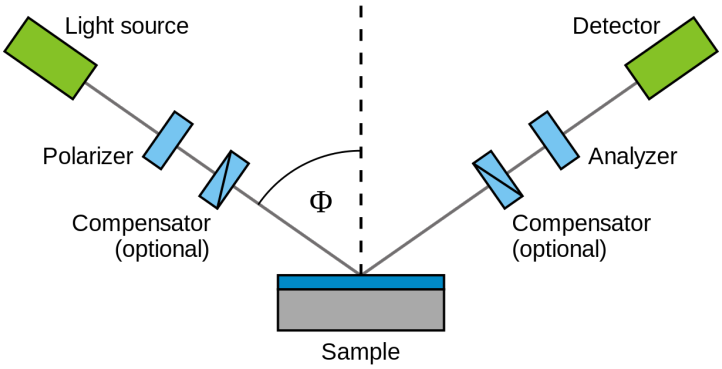

Figure 2.5 – "Ellipsometry setup" by Buntgarn, at the English Wikipedia project. Licensed under CC BY-SA 3.0 via Wikimedia Commons

orientation angels κ. The ray, with fixed polarisation is now reflected from the substrate, and due to the reflection on the three layer system described in section 2.3.1, changes its state of polarization. After the reflection a second linear polariser (called analyser) at angle A, followed by a detector, analyses the beam. P and A are varied to the point where the signal at the detector is minimal. This is the case when the reflected light is linear polarised and extinguished by A, giving this method its name. Since P and A are used to find the minimum this type of Null-Ellipsometry is dubbed PA-Ellipsometry. Using the Jones formalism described in section 2.2.2, all beam altering components can be described via Jones matrices:

$$\text{linear polariser :} \qquad T_{LP}^{te} = K_{LP} \begin{bmatrix} 1 & 0 \\ 0 & 0 \end{bmatrix} \tag{2.3.13}$$

$$\text{compensator (quaterwaveplate) :} \qquad T_{C}^{fs} = K_{C} \begin{bmatrix} 1 & 0 \\ 0 & \delta_C \end{bmatrix} \tag{2.3.14}$$

$$\text{film :} \qquad T_{S}^{xy} = \begin{bmatrix} V_{ex} & 0 \\ 0 & V_{ey} \end{bmatrix}. \tag{2.3.15}$$

Here the indices t, e stand for transmission-, emission-axis of the polariser. f, s for the fast- and slow- axis of the compensator. And x, y build a coordinate system where y is perpendicular to x which lies the plain of incidence.
The Jones matrix describing the entire system can be calculated by multiplying the Jones matrices of all involved components, given that they are rotated into the eigenpolarisation coordinate system of the next component. The detected signal $\mathcal{L}_D$ can than be written as:

$$\mathcal{L}_D = const. \cdot |L|^2 \tag{2.3.16}$$

where L is given by

$$\begin{aligned} L = {} & V_{ex} \cos A \left[\cos C \cos(P - C) - \rho_C \sin C \sin(P - C)\right] \\ & + V_{ey} \sin A \left[\sin C \cos(P - C) + \rho_C \cos C \sin(P - C)\right] \end{aligned} \tag{2.3.17}$$

The detected signal is now dependent on P, C, A, V_{ex} and V_{ey}. For $\mathcal{L} = 0$ the complex reflection ratio ρ_S becomes:

$$\begin{aligned}\rho_s &= \frac{V_{ex}}{V_{ey}} \\ &= -\tan A \frac{\tan C - i\,\tan(P-C)}{1 + i\,\tan C\,\tan(P-C)} \quad .\end{aligned} \tag{2.3.18}$$

For a fixed compensator with $\delta_C = -\frac{\pi}{2}$ at $C = \pm\frac{\pi}{4}$ equation 2.3.18 can be simplified to:

$$\rho_S = \mp \tan A e^{2i(P \mp \pi/4)} \tag{2.3.19}$$

resulting in two pairs of (P', A') that extinguish the beam.

PC-Ellipsometry

If for some reason, such as reduced space or cryogenic temperatures, it is not possible to rotate the analyser, a different approach can be to rotate the polariser and compensator as presented in [Bau13]. With a fixed analyser one degree of freedom is lost, to compensate for this loss, the compensator can be chosen to be rotatable. This allows to generate polarized light with a freely selectable ellipticity angle κ at any given orientation angle ξ. Now a pair of P and C can be found where the intensity of the light is minimal after the fixed analyser at angle A, making it possible to calculate the complex reflection ratio ρ_S.

2.4 Rotating Quaterwave Stokes Polarimeter

The Rotating Quaterwave Stokes Polarimeter (RQP), seen in figure 2.6, is a device that allows to measure the in section 2.1 mentioned Stokes parameters. It is build from a rotatable compensator followed by a fixed polariser. The intensity measured after the compensator at angle α followed by the polariser at angle β can be computed in an analog way to the calculations in section 2.3.2. The Jones matrix for the compensator

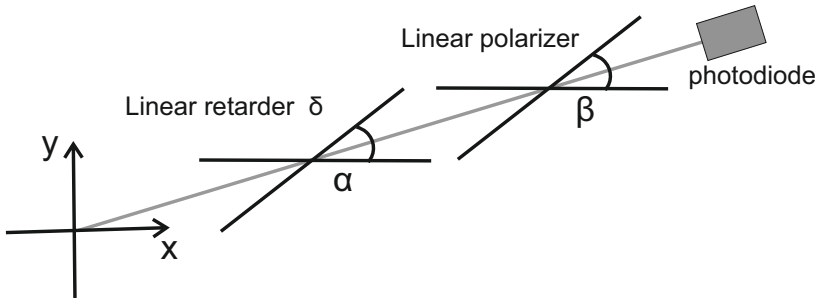

Figure 2.6 – Rotating Quaterwave Stokes Polarimeter. A linear retarder with retardation angle δ and azimuth α is placed in front of a linear polarizer with azimuth β.

described in equation 2.3.14 can be written as a Mueller matrix:

$$\mathrm{M}_{comp}(\delta,\alpha) = \begin{bmatrix} 1 & 0 & 0 & 0 \\ 0 & \cos(4\alpha)\sin^2\left(\frac{\delta}{2}\right) + \cos^2\left(\frac{\delta}{2}\right) & \sin(4\alpha)\sin^2\left(\frac{\delta}{2}\right) & -\sin(\delta)\sin(2\alpha) \\ 0 & \sin(4\alpha)\sin^2\left(\frac{\delta}{2}\right) & \cos^2\left(\frac{\delta}{2}\right) - \cos(4\alpha)\sin^2\left(\frac{\delta}{2}\right) & \sin(\delta)\cos(2\alpha) \\ 0 & \sin(\delta)\sin(2\alpha) & -\sin(\delta)\cos(2\alpha) & \cos(\delta) \end{bmatrix} \tag{2.4.1}$$

where α is the azimuth of the fast axis of the wave plate. The polariser from equation 2.3.13 becomes:

$$\mathrm{P}(\beta) = \frac{1}{2}\begin{bmatrix} 1 & \cos(2\beta) & \sin(2\beta) & 0 \\ \cos(2\beta) & \cos^2(2\beta) & \cos(2\beta)\sin(2\beta) & 0 \\ \sin(2\beta) & \cos(2\beta)\sin(2\beta) & \sin^2(2\beta) & 0 \\ 0 & 0 & 0 & 0 \end{bmatrix}. \tag{2.4.2}$$

The alteration of the incoming beam with Stokes vector $\vec{S}_i$ to the outgoing beam $\vec{S}_o$, can be computed via matrix multiplication of $P(\beta)$ and $M\left(\frac{\pi}{2},\alpha\right)$ (quaterwave plate):

$$\vec{S}_o = \mathrm{P}(\beta)\cdot\mathrm{M}_{\mathrm{comp}}\left(\frac{\pi}{2},\alpha\right)\cdot\vec{S}_i. \tag{2.4.3}$$

For a fixed polariser at angle $\beta = 0°$ the intensity I behind both components can be

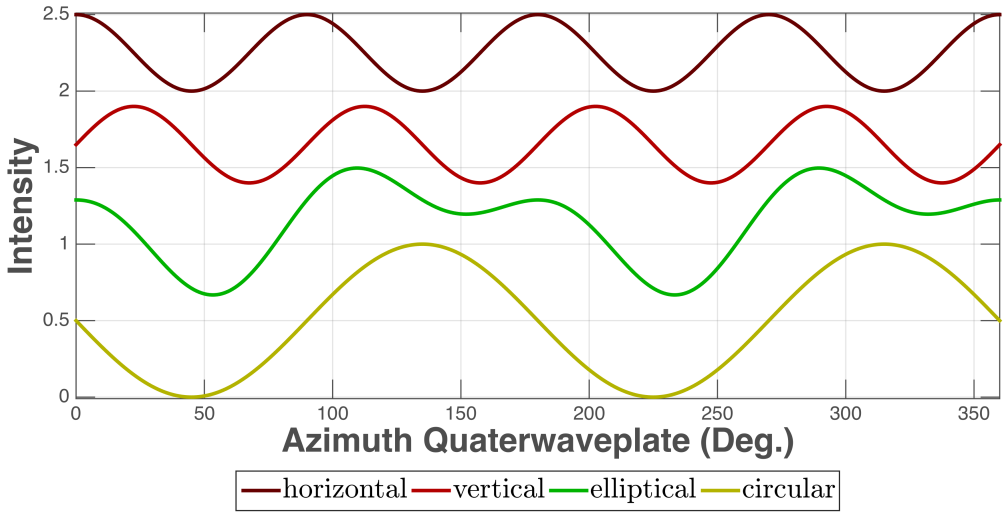

Figure 2.7 – visualization of equation 2.4.4, for four types of polarization with Stokesvectors: ***horizontal*** $\vec{S} = (4, 1, 0, 0)$, ***vertical*** $\vec{S} = (3, 0, 1, 0)$, ***elliptical*** $\vec{S} = (2, \sqrt{1/3}, \sqrt{1/3}, \sqrt{1/3})$ and ***circular*** $\vec{S} = (1, 0, 0, 1)$. All four plots are normed to the intensity caried by the polarisation P, and for better visibility S_0 is different for each graph.

written as a superposition of the four Stokes parameters [Flu08]

$$I\left(\vec{S}, \delta = \frac{\pi}{2}, \alpha, \beta = 0\right) = \frac{S_0}{2} + \frac{S_1}{2}\left(\frac{1}{2} + \frac{1}{2}\cos(4\alpha)\right) + \frac{S_2}{4}\sin(4, \alpha) - \frac{S_3}{2}\sin(2\alpha) \tag{2.4.4}$$

Figure 2.7 shows the four main types of polarization in an example plot.

3 Adapting the PC-Ellipsometry to the new requirements

For the use at the KATRIN-experiment, the CKrS (figure 3.2) has to be adapted to the CPS as described in [Bau13]. The newly designed cold head (figure 3.1) leaves no space for a rotatable analyser. The beam (a) is guided via 2 dielectric mirrors (b,i) towards the substrate (c) where it is reflected. Behind the reflection it passes through a fixed analyser (d), where shortly after the intensity is measured by a photo diode (e).
In this bachelor thesis the ellipsometry, for the new CKrS set up is tested. The main focus of attention will be on investigating the polarisation altering effects of the used mirrors.

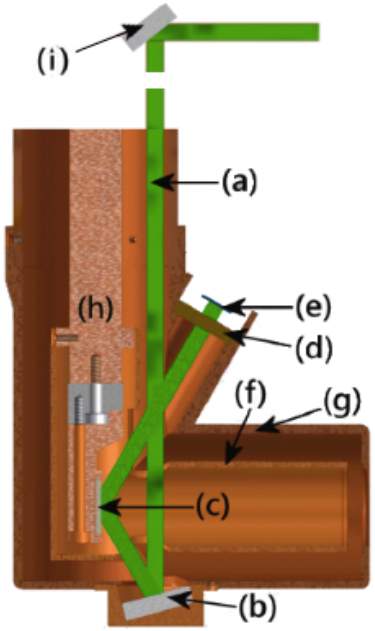

Figure 3.1 – Design of the new cold-head, as presented in [Bau13]. **(a)** beam, **(b)** mirror 15°, **(c)** substrate, **(d)** analyser, **(e)** detector, **(f)** inner coldshield, **(g)** outer coldshield and **(i)** mirror 45°

3.1 Testing the mirrors

Since ellipsometry is highly sensitive to changes in polarization, it is necessary, that the mirrors used maintain the ingoing polarization as good as possible. During the master thesis of Anne Wegman [Weg10] different types of mirrors were tested, because of their good properties it was decided to use dielectric mirrors. Daniel Spitzer tested the ellipsometry via two dielectric mirrors with an reflection angle of 45°

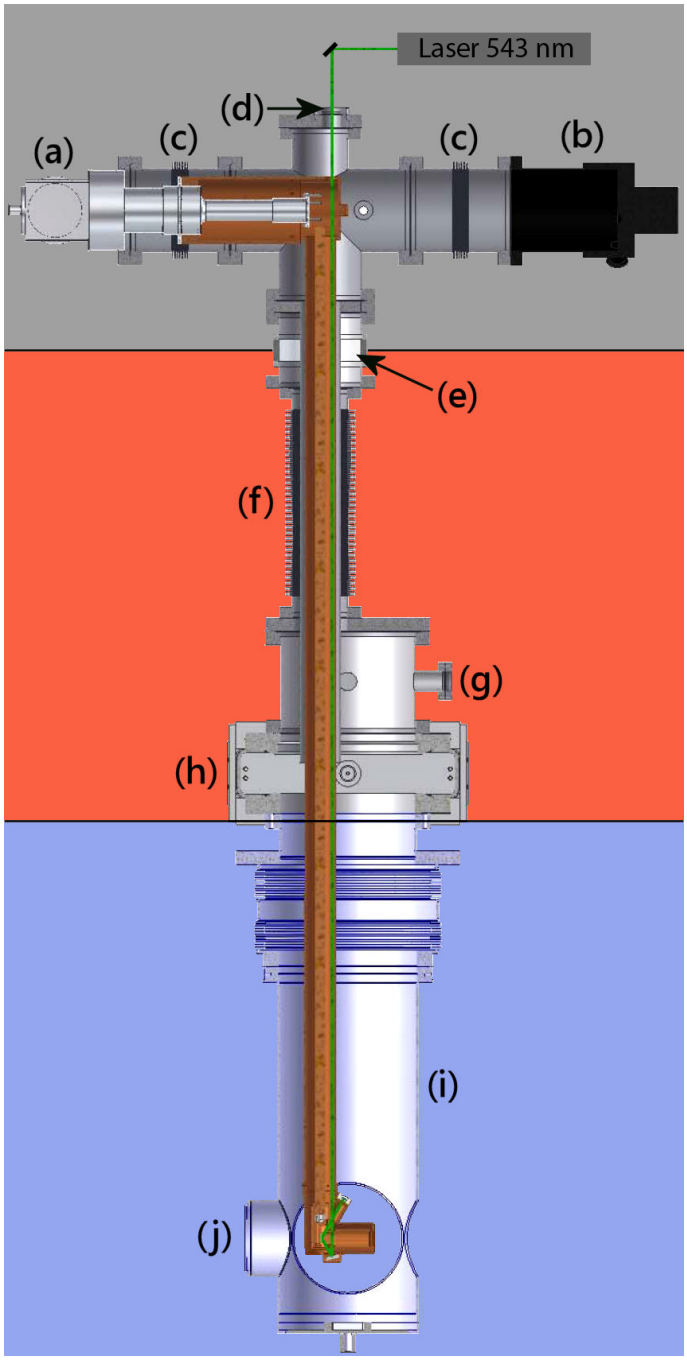

Figure 3.2 – "Side view of the CKrS at the CPS. The CKrS is divided into the section on high volt- age (gray) and the grounded part (red). Both are connected on top of the CPS (blue). The top part consists of the cryocooler **(a)**, the TMP **(b)** both are connected via bellows **(c)** to reduce vibrations. The laser beam will be guided through a window on the top **(d)**. The insulation between the high voltage and the grounded part is done by a ceramic insulator **(e)**. To enable the vertical movement the insulator and the ablation chamber **(g)** are connected via a bellows **(f)**. The separation between the CKrS and the CPS is done by a CF250 gate valve **(h)**. The CKrS enters the pump port 2 **(i)**and scans the flux tube inside the beam tube **(j)**." [Bau13]

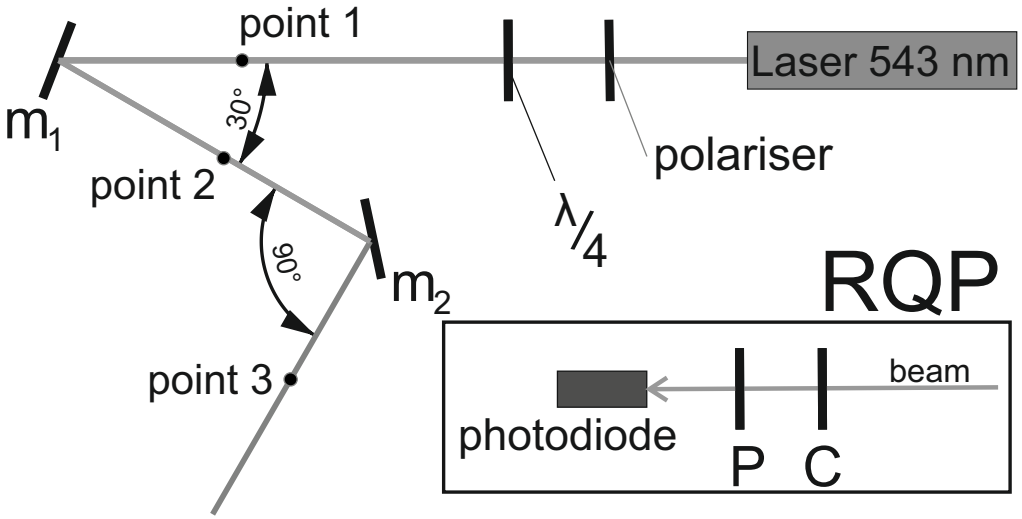

Figure 3.3 – Test set up for mirrors. A green HeNe-Laser followed by a adjustable polariser and compensator produce polarized light. The polarisation can then be measured, using the RQP at three different points.

and concluded that despite slight losses in resolution, it is possible [Spi11].
The new design requires two additional mirrors, one to deflect the laser beam by 90° into the cold finger of the new CKrS and the other one for the 30° reflection onto the substrate (figure 3.1 (b)). The mirrors are tested and compared to the ones tested in Daniel Spitzers Master thesis, with the set up shown in figure 3.3 are.

3.1.1 Set Up

In order to compare the mirrors m_1 (15° angle of reflection)[1] and m_2 (45° angle of reflection)[2] a RQP[3] as seen in figure 3.3 was build. The compensator is a waveplate with $\delta = \frac{\pi}{2}$. Both, polariser and compensator are mounted on rotation stages[4], with a unidirectional angle resolution of 50 μrad. For each measurement, the polarisation of the beam is prepared, via a combination of a manually adjustable polariser followed by a

[1]Mirror 1, Laseroptik, custom made, batch no. 01041Wi1
[2]Mirror 2, Laseroptik, conventional, model no. L-00217
[3]Polariser : PGT 2.05 Bernhard Halle Nachfolger GmbH - optische Werkstaetten
Compensator : CVI Melles Griot QWPM-543-04-4-R10
[4]*PI*, Model: M-060.DG

quaterwaveplate[5]. The polarization is measured before (point 1) and after the reflection at m_1 (point 2) and behind m_2 (point 3) using a RQP. The light source consists of a green He-Ne-Laser[6] followed by a combination of polariser and quaterwaveplate, producing left handed circular polarized light. The detector is a Si-Pin-diode[7] which is amplified[8] by a factor 10^4 and than digitalised via a 12 bit ADC[9]. The ADC is read out via *Labview*. This set up allows to analyse each mirror individually and in combination.

3.1.2 Measurement of polarisation stability

27 measurements with nine different types of polarizations are made to characterize the polarization altering features of said mirrors. Each polarization is given a number:

No.	**expected polarization**
1	circular polarized beam
2, 3	linear p- and s-polarized
4	linear at 45°
5, 6	elliptical polarized light with $\kappa \approx \frac{\pi}{8}$, $\xi \approx \frac{\pi}{4}, \frac{3\pi}{4}$
7 − 9	elliptical polarized light[10]

The data is then fitted with function 2.4.4 the goodness of the fits is given by the root mean square error (RMSE).

$$SSE = \frac{1}{n}\sum_{i=1}^{n}(y_i - \hat{y}_i)^2$$
$$MSE = \frac{SSE}{v}$$
$$RMSE = \sqrt{MSE}$$

where v is the number of residual degrees of freedom. A value closer to zero indicates a fit that is more useful for prediction. After the measurements it was discovered, that the

[5] for linear polarized light only the polariser was used.
[6] *Thorlabs*, Model no. HGP005-1
[7] *Hamamatsu, type S-3590-19*
[8] *Femto*, type: DLPCA-200
[9] *NI*, type: USB-6008
[10] The light was prepared with PC-pairs measured for thin films taken from the ellipsometry paper [BGS+13] (Table 3).

polariser was set to $5.86° \pm 0.01°$, making it necessary to correct the measured stokes parameters using the corrections given in [Flu08]:

$$\begin{aligned} S_0(\alpha) &= S_0 + S_2 \sin(2\alpha) \\ S_1(\alpha) &= S_1 \cos(2\alpha) - S_2 \sin(2\alpha) \\ S_2(\alpha) &= S_2 \cos(2\alpha) + S_1 \sin(2\alpha) \\ S_3(\alpha) &= S_3 \cos(2\alpha) \end{aligned} \tag{3.1.1}$$

The figures 3.4-3.8 and I.1-I.4 show the collected data. In each plot the marker corresponds with the position the measurement was taken.

- $\bullet$ before reflection (point 1)
- $*$ after 15° reflection (point 2)
- $\circ$ after 45° reflection (point 3)

The normed Stokes parameters are calculated from the fit parameters, where the systematic error, caused by the uncertainty in the azimuth of the polariser and compensator, is estimated using the corrections given in equation 3.1.1. Due to unstable light conditions inside the laboratory the background in each measurement may vary, causing slight changes in the amplitude of S_0 between measurements, depending on the orientation of the photo diode towards different light sources. Since other people needed to use the laboratory during the measurements, it was not possible to measure a stable background. Fitparameter figure 3.4

$$\begin{pmatrix} -2.4955 \pm 0.0251 \\ 0.0535 \pm 0.0407 \\ -0.0313 \pm 0.0410 \\ -2.4218 \pm 0.0205 \end{pmatrix}^{\circ} \xrightarrow{15°} \begin{pmatrix} -2.4994 \pm 0.0255 \\ 0.0442 \pm 0.0414 \\ -0.0333 \pm 0.0417 \\ 2.4607 \pm 0.0209 \end{pmatrix}^{*} \xrightarrow{45°} \begin{pmatrix} -2.3473 \pm 0.0236 \\ -0.0279 \pm 0.0383 \\ -0.2829 \pm 0.0386 \\ -2.2891 \pm 0.0193 \end{pmatrix}^{\bullet}$$

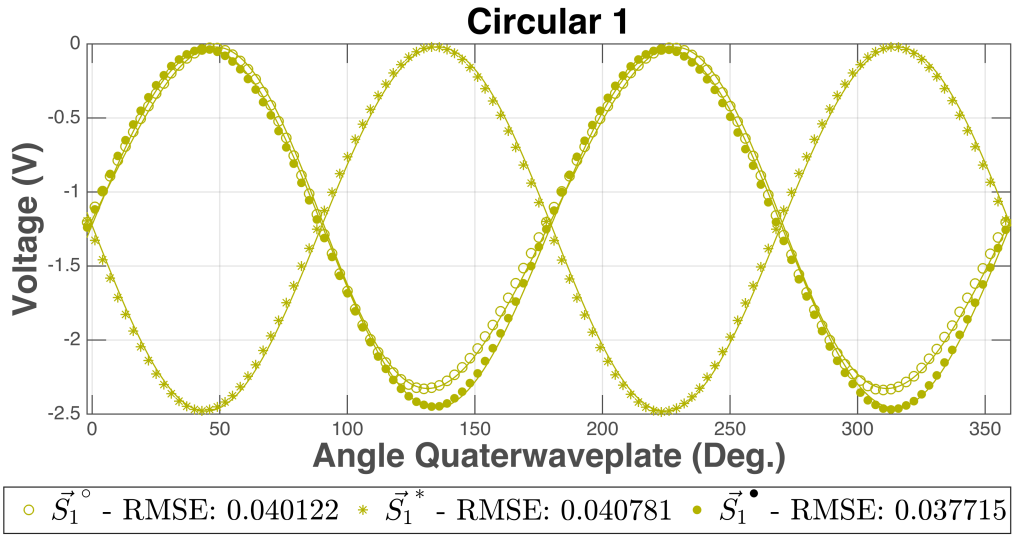

Figure 3.4 – measurement 1, circular polarized light.

Normed and corrected Stokes vectors for 3.4

$$\begin{pmatrix} -1.0547 \pm 0.0256 \\ 0.0248 \pm 0.0172 \\ -0.0083 \pm 0.0173 \\ -0.9997 \pm 0.0242 \end{pmatrix}^{\circ} \xrightarrow{15^{\circ}} \begin{pmatrix} -1.0399 \pm 0.0253 \\ 0.0208 \pm 0.0172 \\ -0.0098 \pm 0.0173 \\ 0.9997 \pm 0.0242 \end{pmatrix}^{*} \xrightarrow{45^{\circ}} \begin{pmatrix} -1.0644 \pm 0.0235 \\ 0.0133 \pm 0.0169 \\ -0.1251 \pm 0.0173 \\ -0.9921 \pm 0.0223 \end{pmatrix}^{\bullet} \tag{3.1.2}$$

Figure 3.4 shows the measurements for right handed circular polarized light. After each reflection the graph seems to be mirrored at the x-axis. The normed Stokes vectors given in 3.1.2 show a change of sign in the S_3 component, meaning that after each reflection right handed circular polarized light becomes left handed circular polarized and vice versa.

Fitparameter figure 3.5

$$\begin{pmatrix} -2.5141 \pm 0.0058 \\ -2.4160 \pm 0.0095 \\ 0.6922 \pm 0.0095 \\ -0.0017 \pm 0.0048 \end{pmatrix}^{\circ} \xrightarrow{15^{\circ}} \begin{pmatrix} -2.4176 \pm 0.0035 \\ -2.3802 \pm 0.0057 \\ 0.6169 \pm 0.0057 \\ -0.0155 \pm 0.0029 \end{pmatrix}^{*} \xrightarrow{45^{\circ}} \begin{pmatrix} -2.2493 \pm 0.0032 \\ -2.1495 \pm 0.0052 \\ 0.6094 \pm 0.0053 \\ -0.0024 \pm 0.0026 \end{pmatrix}^{\bullet}$$

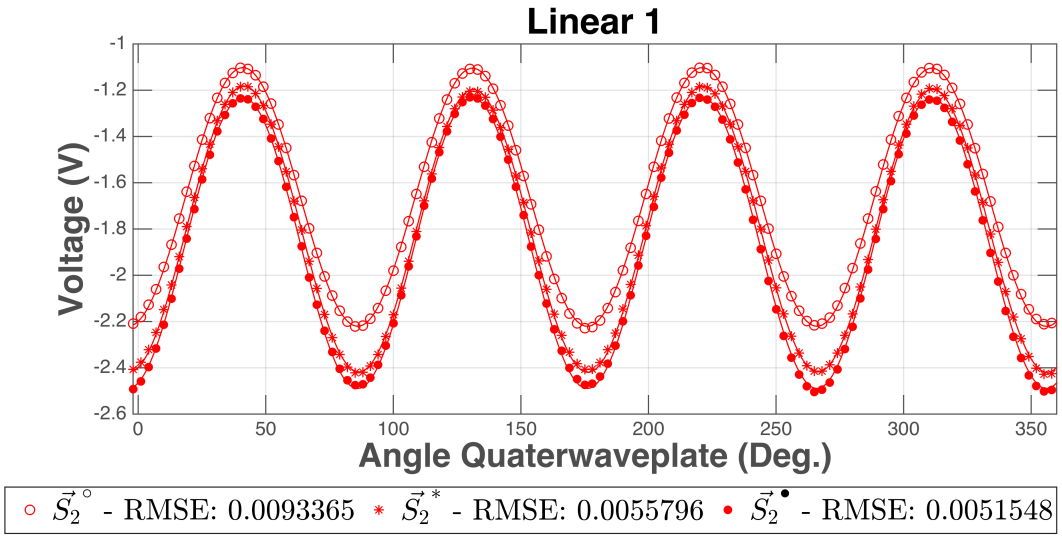

Figure 3.5 – measurement 2, p-polarized.

Normed and corrected Stokes vectors for 3.5

$$\begin{pmatrix} -0.9444 \pm 0.0379 \\ -0.9972 \pm 0.0366 \\ 0.0744 \pm 0.0111 \\ -0.0006 \pm 0.0019 \end{pmatrix}^{\circ} \xrightarrow{15^{\circ}} \begin{pmatrix} -0.9323 \pm 0.0295 \\ -0.9988 \pm 0.0291 \\ 0.0490 \pm 0.0079 \\ -0.0062 \pm 0.0012 \end{pmatrix}^{*} \xrightarrow{45^{\circ}} \begin{pmatrix} -0.9513 \pm 0.0319 \\ -0.9974 \pm 0.0305 \\ 0.0716 \pm 0.0089 \\ -0.0011 \pm 0.0012 \end{pmatrix}^{\bullet} \tag{3.1.3}$$

The measurements given in figure 3.5-3.7 show linear polarized light, with the special cases of s-polarized light in 3.5 and p-polarized light in 3.6. The measurements for s- and p-polarized light show only slight deviations after each reflection, the change in amplitude is probably caused by parasitic light sources in the lab.
Fitparameter figure 3.6

$$\begin{pmatrix} -12.4848 \pm 0.0090 \\ 11.5263 \pm 0.0146 \\ -3.2831 \pm 0.0147 \\ 0.0004 \pm 0.0073 \end{pmatrix}^{\circ} \xrightarrow{15^{\circ}} \begin{pmatrix} -12.0832 \pm 0.0163 \\ 11.5416 \pm 0.0265 \\ -2.8891 \pm 0.0267 \\ -0.0004 \pm 0.0133 \end{pmatrix}^{*} \xrightarrow{45^{\circ}} \begin{pmatrix} -11.9676 \pm 0.0082 \\ 10.9536 \pm 0.0133 \\ -3.1223 \pm 0.0134 \\ 0.0030 \pm 0.0067 \end{pmatrix}^{\bullet}$$

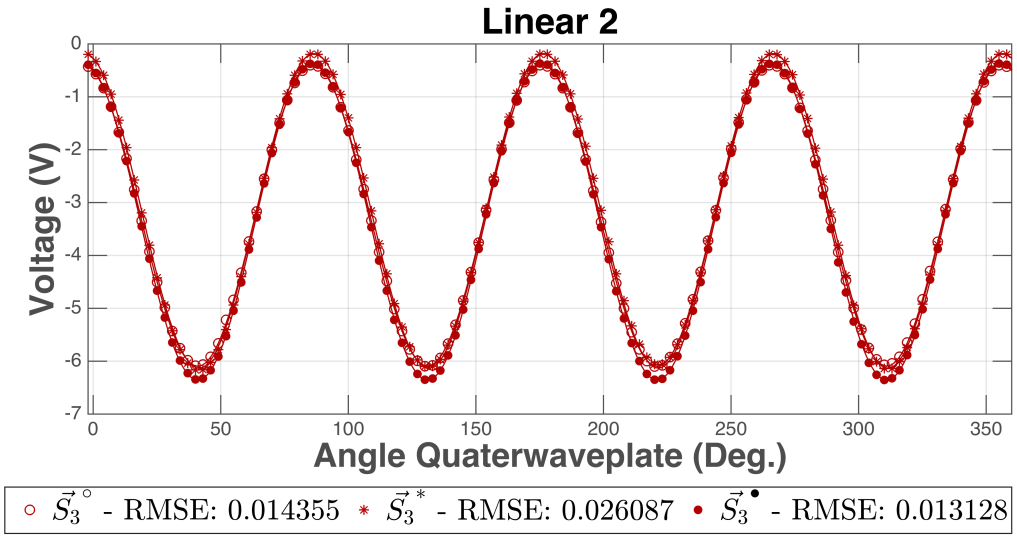

Figure 3.6 – measurement 3, s-polarized.

Normed and corrected Stokes vectors for 3.6

$$\begin{pmatrix} -1.0974 \pm 0.0103 \\ 0.9973 \pm 0.0096 \\ -0.0729 \pm 0.0030 \\ 0.0000 \pm 0.0006 \end{pmatrix}^{\circ} \xrightarrow{15^{\circ}} \begin{pmatrix} -1.0649 \pm 0.0137 \\ 0.9992 \pm 0.0132 \\ -0.0407 \pm 0.0040 \\ -0.0000 \pm 0.0011 \end{pmatrix}^{*} \xrightarrow{45^{\circ}} \begin{pmatrix} -1.1064 \pm 0.0105 \\ 0.9973 \pm 0.0096 \\ -0.0731 \pm 0.0030 \\ 0.0003 \pm 0.0006 \end{pmatrix}^{\bullet} \tag{3.1.4}$$

Fitparameter figure 3.7

$$\begin{pmatrix} -1.3137 \pm 0.0016 \\ 0.3317 \pm 0.0026 \\ 1.1667 \pm 0.0026 \\ 0.0010 \pm 0.0013 \end{pmatrix}^{\circ} \xrightarrow{15^{\circ}} \begin{pmatrix} -1.2183 \pm 0.0013 \\ -0.3001 \pm 0.0021 \\ -1.1940 \pm 0.0021 \\ -0.0232 \pm 0.0010 \end{pmatrix}^{*} \xrightarrow{45^{\circ}} \begin{pmatrix} -1.2236 \pm 0.0025 \\ 0.3066 \pm 0.0040 \\ 1.0723 \pm 0.0040 \\ -0.1121 \pm 0.0020 \end{pmatrix}^{\bullet}$$

Normed and corrected Stokes vectors for 3.7

$$\begin{pmatrix} -0.8877 \pm 0.0062 \\ 0.0724 \pm 0.0026 \\ 0.9974 \pm 0.0058 \\ 0.0008 \pm 0.0011 \end{pmatrix}^{\circ} \xrightarrow{15^{\circ}} \begin{pmatrix} -1.1864 \pm 0.0037 \\ -0.0417 \pm 0.0019 \\ -0.9990 \pm 0.0039 \\ -0.0185 \pm 0.0008 \end{pmatrix}^{*} \xrightarrow{45^{\circ}} \begin{pmatrix} -0.8975 \pm 0.0090 \\ 0.0735 \pm 0.0042 \\ 0.9925 \pm 0.0085 \\ -0.0980 \pm 0.0020 \end{pmatrix}^{\bullet} \tag{3.1.5}$$

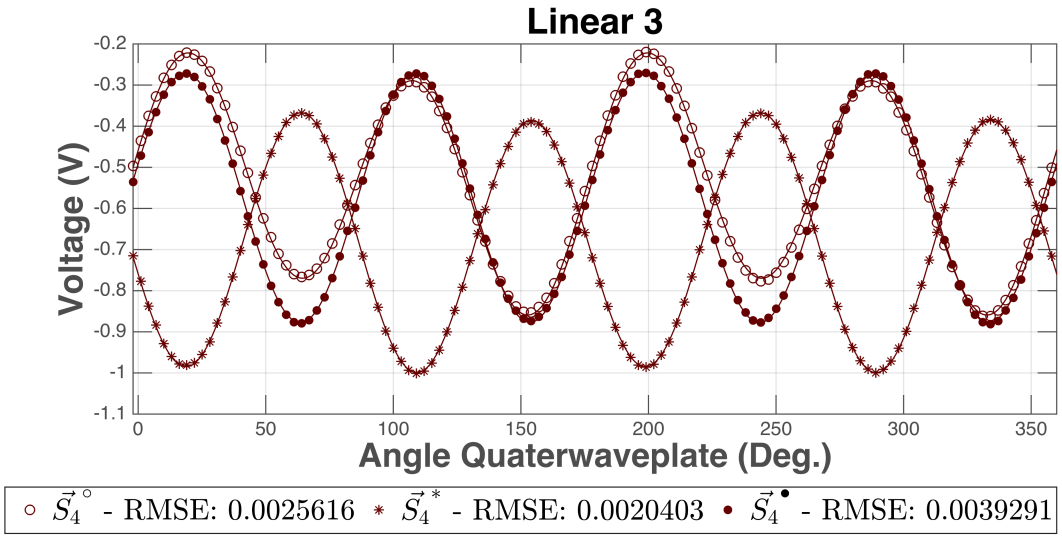

Figure 3.7 – measurement 4, linear polarized (45°)

Figure 3.7 shows linear polarized light at an angle of approximately 45°. Similar to figure 3.6 the measurements seem to be mirrored at the x-axis after each reflection. S_2 changes its sign after each reflection causing a 90° shift in polarization angle ξ.

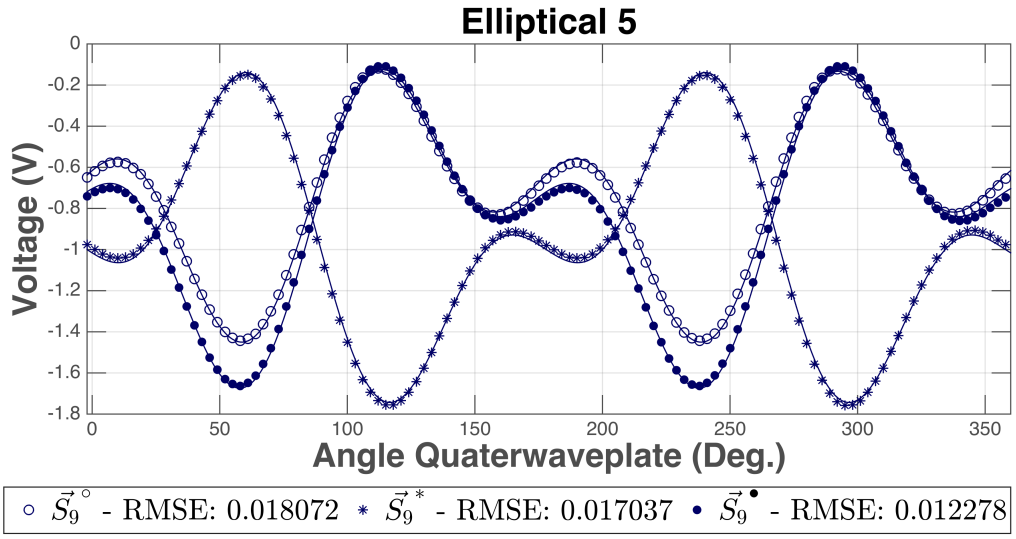

Figure 3.8 – measurement 9, elliptically polarized.

Fitparameter figure 3.8

$$\begin{pmatrix} -1.9726 \pm 0.0113 \\ 0.5651 \pm 0.0183 \\ 1.4201 \pm 0.0185 \\ 1.0287 \pm 0.0092 \end{pmatrix}^{\circ} \xrightarrow{15^{\circ}} \begin{pmatrix} -1.8170 \pm 0.0107 \\ -0.2151 \pm 0.0173 \\ -1.5224 \pm 0.0174 \\ -1.0778 \pm 0.0087 \end{pmatrix}^{*} \xrightarrow{45^{\circ}} \begin{pmatrix} -1.7657 \pm 0.0077 \\ 0.5341 \pm 0.0125 \\ 1.3699 \pm 0.0126 \\ 0.7751 \pm 0.0063 \end{pmatrix}^{\bullet}$$

Normed and corrected Stokes vectors for 3.8

$$\begin{pmatrix} -0.9201 \pm 0.0284 \\ 0.1447 \pm 0.0128 \\ 0.8223 \pm 0.0224 \\ 0.5503 \pm 0.0153 \end{pmatrix}^{\circ} \xrightarrow{15^{\circ}} \begin{pmatrix} -1.1402 \pm 0.0186 \\ 0.0529 \pm 0.0095 \\ -0.8228 \pm 0.0175 \\ -0.5659 \pm 0.0115 \end{pmatrix}^{*} \xrightarrow{45^{\circ}} \begin{pmatrix} -0.8989 \pm 0.0226 \\ 0.1479 \pm 0.0101 \\ 0.8762 \pm 0.0187 \\ 0.4587 \pm 0.0104 \end{pmatrix}^{\bullet} \quad (3.1.6)$$

Figure 3.8 and I.1-I.4 show the case for ellipical polarized light. Again the graphs seem to be mirrored along the x-Axis. S_2 and S_3 both change their signs between each reflection, changing the rotation direction of the ellipse.
Figure 3.9 shows all measurements on a Poincare sphere. With the exception of p- and s-polarized light, all measurements change the hemisphere after reflection. This change can be explained with the phase shift of π for s-polarized light after reflection(figure 2.3). p-polarized light does not experience this variation, causing a change in polarisation. The switching of sign in S_2 and S_3 can be explained by this phase shift for s-polarised light. Since this set up does not allow to measure the absolute phase of the ray, no significant alterations for purely s-polarized light can be observed.

3.2 Correcting polarization altering effects of used mirrors

In order to correct the polarisation altering effects of the mirrors, an attempt was made to find a Mueller matrix that describes this change in polarisation. To keep the normalisation of an ingoing Stokes vector the Mueller matrix is build from a sequence of two rotations. Since S_1 does not change its sign after reflection, the first rotation of approximately 180° is made around S_1, followed by a smaller rotation around S_3. The rotations can be

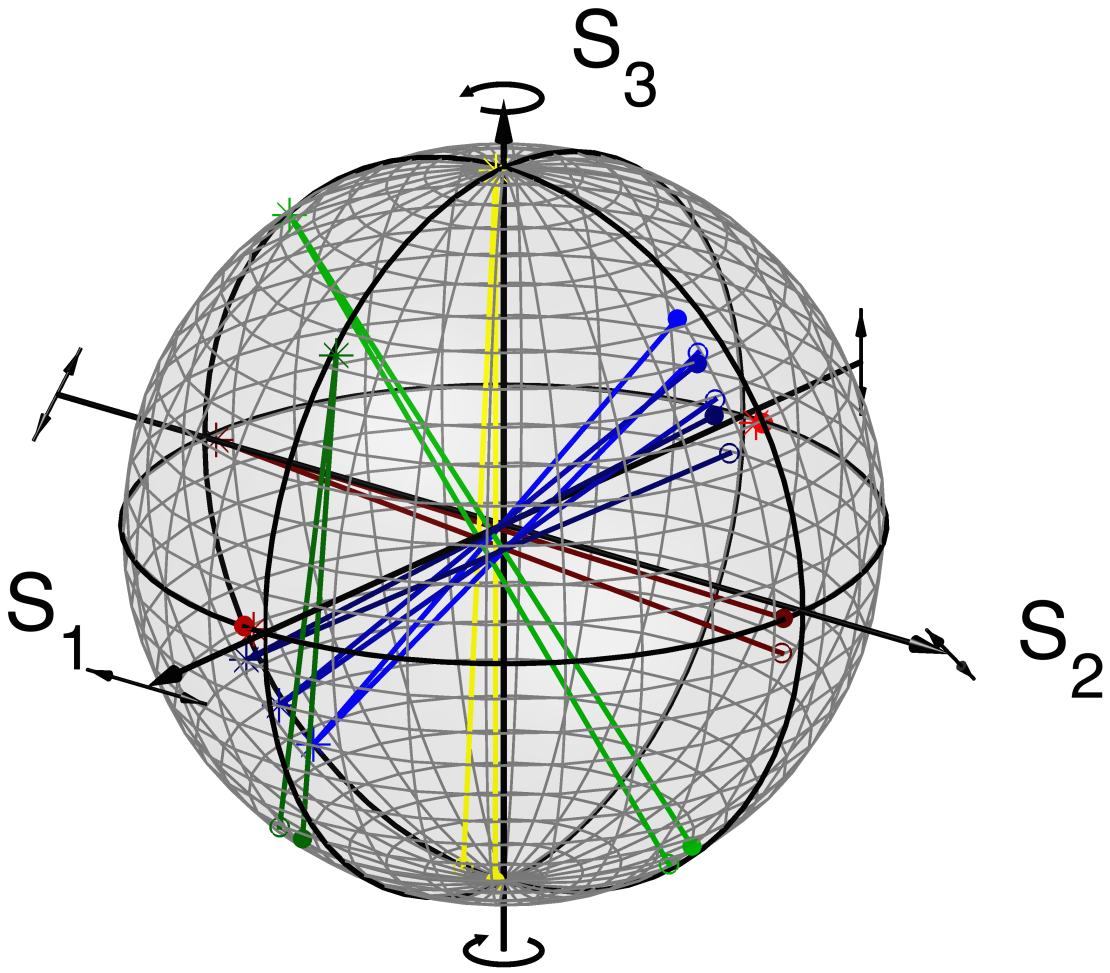

Figure 3.9 – Mesurements 1-9 displayed on a Poincaresphere. The colors correspond with the colors in figures 3.4-3.8, and I.1-I.4.

calculated via:

$$\mathrm{M}_{S_1}(\gamma_i) = \begin{bmatrix} 1 & 0 & 0 & 0 \\ 0 & \cos\gamma_i & -\sin\gamma_i & 0 \\ 0 & \sin\gamma_i & \cos\gamma_i & 0 \\ 0 & 0 & 0 & 1 \end{bmatrix} \quad \mathrm{M}_{S_3}(\nu_i) = \begin{bmatrix} 1 & 0 & 0 & 0 \\ 0 & 1 & 0 & 0 \\ 0 & 0 & \cos\nu_i & -\sin\nu_i \\ 0 & 0 & \sin\nu_i & \cos\nu_i \end{bmatrix}. \tag{3.2.1}$$

With $i = 1, 2$. γ_i and ν_i are altered to the point, where the median D_{av} (equation 3.2.3) of the overlap $\vec{S}_{\mathrm{out}_i}$ and the corrected incoming beam $\vec{S}_{\mathrm{rot}_i}$ is best for all nine measured polarisations.

$$\vec{S}_{\mathrm{rot}_i} = \mathrm{M}_{S_1}(\gamma_i) \cdot \mathrm{M}_{S_3}(\alpha_i) \cdot S_{\mathrm{in}_i} = \mathrm{M}_i(\gamma_i, \alpha_i) \cdot \vec{S}_{\mathrm{in}_i} \tag{3.2.2}$$

Defining D_{av} as:

$$D_{\mathrm{av}} = \sum_{k=1}^{9} \arccos\left(\vec{S}_{\mathrm{out}_k} \cdot \vec{S}_{\mathrm{rot}_k}(\gamma_i, \nu_i)\right) \tag{3.2.3}$$

γ_i and ν_i can be altered and a minimal value in the γ-ν-plane can be found (figure 3.10). Blue colors indicate a small distance, meaning a good overlap, while yellow colors indicate a bad overlap. The pair with the best overlap is then chosen to calculate the Mueller matrix for each mirror. The found rotation angles can be seen in table 3.1

mirror	reflection angle	γ	ν
1	15°	$172.73° \pm 0.01°$	$6.82° \pm 0.01°$
2	45°	$181.04° \pm 0.01°$	$6.52° \pm 0.01°$

Table 3.1 – Rotation angles found from figure 3.10

Since at the CKrS both mirrors will be used, a combination of matrices M_1 and M_2 can be computed. This matrix will allow to correct the polarisation altering effects caused by the combination of both mirrors:

$$\mathrm{M}_{\mathrm{tot}}(\gamma_1, \gamma_2, \nu_1, \nu_2) = \mathrm{M}_1(\gamma_2, \nu_2) \cdot \mathrm{M}_2(\gamma_1, \nu_1) \tag{3.2.4}$$

Figure 3.11 shows the polarisation measured before (black) and after the reflection at both mirrors (red). Using the matrix given in equation 3.2.4 a prediction of the outcoming

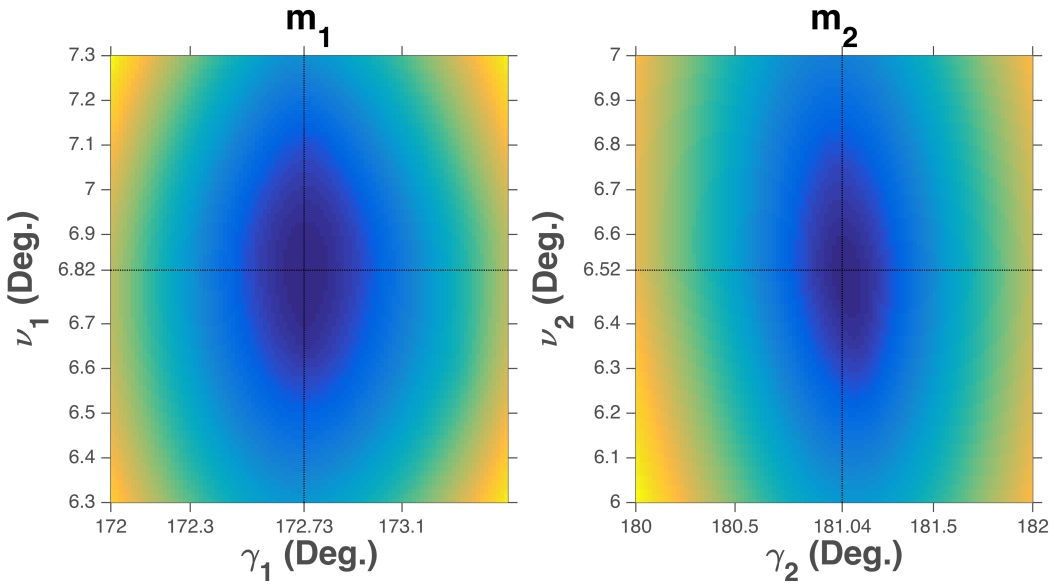

Figure 3.10 – D_{av} plotted against γ and ν. regions in blue indicate good overlap (small distance on sphere), regions in yellow show a bad overlap.

polarisation $\vec{S}_{\mathrm{p}}$ of an incoming beam $\vec{S}_{\mathrm{in}}$ is made (blue).

$$\vec{S}_{\mathrm{p}} = \mathrm{M}_{\mathrm{tot}} \cdot \vec{S}_{\mathrm{in}} \tag{3.2.5}$$

Figure 3.12 shows the distance between $\vec{S}_{\mathrm{p}}$ and $\vec{S}_{\mathrm{in}}$ to $\vec{S}_{\mathrm{out}}$. It can be seen, that the distance between $\vec{S}_{\mathrm{p}}$ and $\vec{S}_{\mathrm{out}}$ with an average value of 0.0098 ± 0.0047 is about one order of magnitude smaller than the distance between $\vec{S}_{\mathrm{in}}$ and $\vec{S}_{\mathrm{out}}$ (0.0815 ± 0.0462), this indicates a good understanding of the polarisation state after the mirrors.

3.2.1 Comparing m_1 and m_2

Since Daniel Spitzer allready showed, that the ellipsometry via two mirrors, of the same type as m_2, is possible [Spi11], the mirrors m_1 and m_2 will be compared to each other. If m_1 has better properties than m_2, ellipsometry via a combination of both should be possible. During the measurements the CKrS was not fully operational, making it impossible to measure a krypton-reference-curve as presented in [Spi11] to compare the quality of the mirrors.

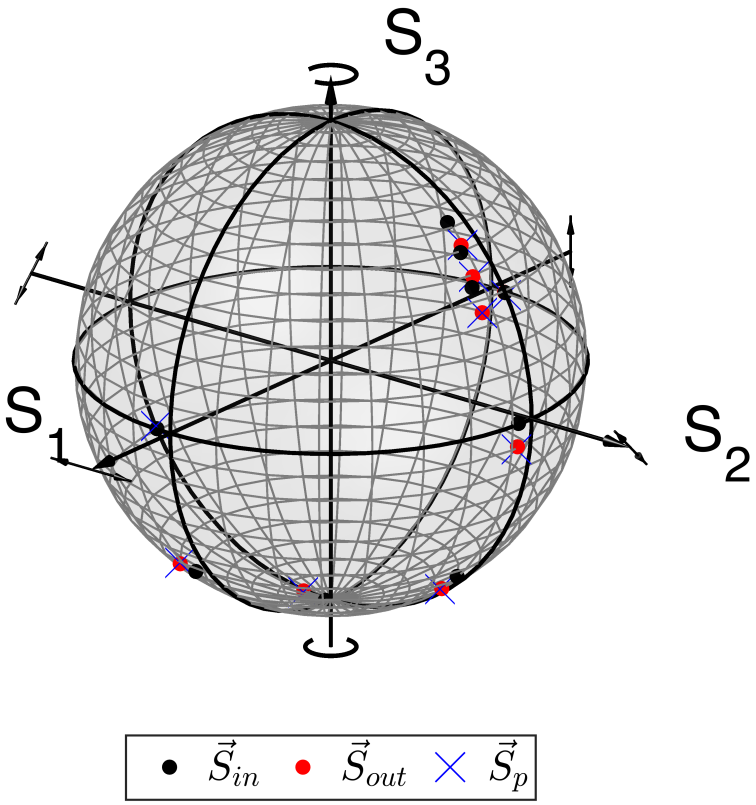

Figure 3.11 – The polarisation of light before (black) and after reflection at $m_1 + m_2$ (red) compared to the predicted polarisation (blue) on a Poincare sphere.

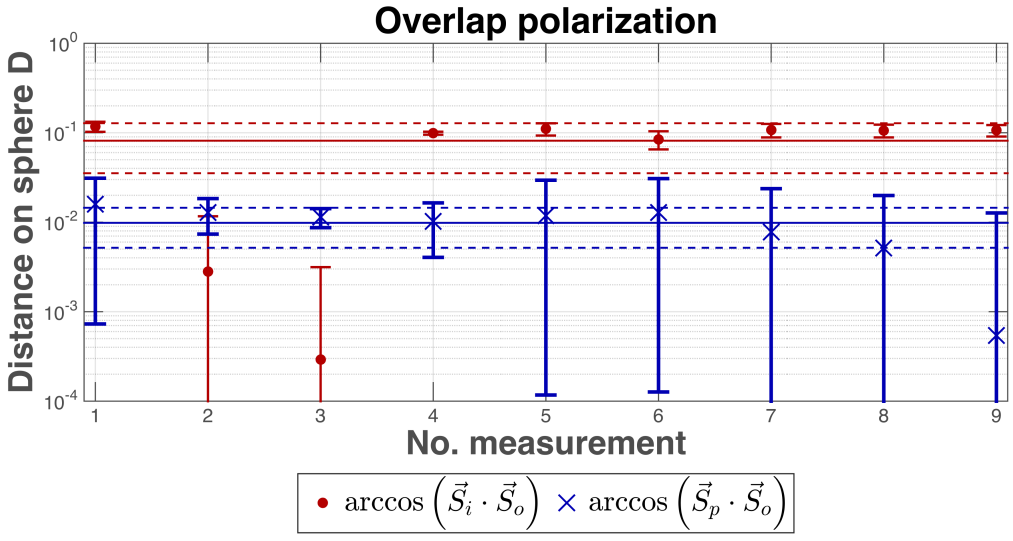

Figure 3.12 – The overlap of S_{in} with S_{out} and S_p. The corrected stokes vector $\vec{S}_p$ is about one order of magnitude closer to $\vec{S}_i$ than the uncorrected $\vec{S}_{out}$

A different approach to compare the mirrors, can be to analyse their Mueller matrices. For perfect dielectric mirrors[11] the Mueller matrix describing the total transition of two reflections should be the identity matrix I_4. By multiplying the Mueller matrix of each mirror with it self, and comparing it to the identity matrix, the quality of the mirrors can be compared. With

$$A = \mathrm{M}_1 \cdot \mathrm{M}_1 \qquad \text{and} \qquad B = \mathrm{M}_2 \cdot \mathrm{M}_2 \tag{3.2.6}$$

The "similarity" D_{M_i} to the identity matrix of the Muller matrices can be defined as:

$$D_{M_1} = \sum_{i=1}^{4}\sum_{j=1}^{4} |\mathrm{I}_{ij} - A_{ij}| \qquad D_{M_2} = \sum_{i=1}^{4}\sum_{j=1}^{4} |\mathrm{I}_{ij} - B_{ij}| \tag{3.2.7}$$

where a value closer to zero indicates a smaller change in polarization. Using equation 3.2.7 the "similarity" can be calculated:

$$D_{M_1} = 0.0786 \qquad D_{M_2} = 0.5978 \quad . \tag{3.2.8}$$

D_{M_1} is a factor of 7.6 more "similar" to to the identity matrix than D_{M_2}, showing that the mirror with a 15° reflection angle changes the polarization less than the mirrors tested in [Spi11]. For the combination of both mirrors $D_{M_{1,2}}$ the same approach results in a value of

$$D_{M_{1,2}} = 0.2446 \tag{3.2.9}$$

which is still a factor of 2.4 more "similar" than the combination of two 45° mirrors.

3.2.2 Testing corrections on ellipsometry measurements

An ellipsometry set up[12] with the same mirror sequence as in the new CKrS (figure 3.13) is build to test the ellipsometry in a more realistic setting. Due to technical constraints it was not possible to build the set up with the same path length as in the final CKrS ($\approx 2\,\mathrm{m}$), in the here presented set up the path is approximately 3.5 m long. The laser

[11] Taking a phaseshift of π for s-polarized light into account.
[12] The same laser and optical instruments as in the RQP-set-up is used

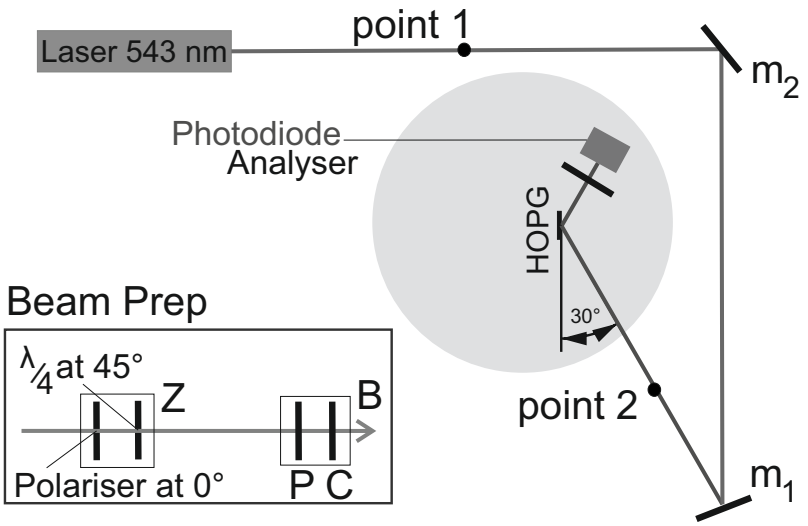

Figure 3.13 – Set up to test the ellipsometry via m_2 and m_1. The "Beam Prep" consists of a section Z (Linear polariser at 0° followed by a quarter waveplate at 45°) that turns the laser into fully circular polarised light and a section B that consists of a rotatable polariser at angle P and compensator at angle C. P and C can be varied to the point where the intensity measured at the photo diode is minimal. By positioning the Beam Prep at point 1 and point 2, ellipsometry measurements with and without mirrors can be made and compared.

is mounted next to the vacuum chamber, facing in the same direction as the normal of the HOPG[13]. m_2 is located approximately 1 m behind the laser. After the reflection the beam passes a distance of ≈ 1.5 m where it hits m_1. Two pinholes[14] with a gap of 30 cm between each other are placed in front of the vacuum chamber inlet. The two pinholes enable to align the laser between different set ups, reducing the error caused by different orientations of the ray. After the pinholes, approximately 1 m distance to m_1, the ray is reflected at the HOPG and passes through the analyser[15].

Two ellipsometry measurements, on a warm (23° C) HOPG, one with the Beam Prep at point 1 the other at point 2 are made. A *Labview vi* presented in [Weg10] is used to find an approximate minimum in the PC-plane, afterwards an area of $20° \times 20°$ around this minimum is scanned in 0.25° steps to find a more accurate minimum. From the point of minimal intensity the complex reflection ratio ρ_s of the HOPG can be derived via equation 2.3.18. Using Mueller calculus as explained in section 2.1.1, the polarisation of

[13] grade SPI-2, SPI Supplies
[14] The first pinhole a a diameter of 3 mm, the second a diameter of 2 mm
[15] A polariser at 30° - Thorlabs LPVISB050, not laminated

the ingoing beam can be determined from the PC-pair by

$$\vec{S} = \mathrm{M}_{\mathrm{comp}}\left(C, \frac{\pi}{2}\right) \cdot \mathrm{P}(P) \cdot \vec{S}_{\mathrm{circ}} \tag{3.2.10}$$

where $\vec{S}_{\mathrm{circ}}$ is the normed Stokes vector for left hand circular polarized light (table 2.1). Using this equation a stokes vector $\vec{S}'_{\mathrm{mirror/nomirror}}$ for each pair is calculated. The measurement with mirrors is then corrected using the Mueller matrices from section 3.2. Since the mirror sequence is different to the one used with the RQP a new Mueller matrix can be calculated via:

$$\mathrm{M}_{elli}(\gamma_1, \gamma_2, \nu_1, \nu_2) = \mathrm{M}_1(\gamma_1, \nu_1) \cdot \mathrm{M}_2(\gamma_2, \nu_2). \tag{3.2.11}$$

The calculated Stokes vectors are:

$$\vec{S}_{\mathrm{nomirror}} = \begin{pmatrix} 1 \\ -0.3826 \\ -0.7407 \\ 0.5522 \end{pmatrix} \qquad \vec{S}_{\mathrm{mirror}} = \begin{pmatrix} 1 \\ -0.3856 \\ -0.7856 \\ 0.4839 \end{pmatrix} \quad . \tag{3.2.12}$$

The corrected stokes vector can be calculated via:

$$\vec{S}_{\mathrm{corrected}} = M_{\mathrm{elli}} \cdot \vec{S}_{\mathrm{mirror}} = \begin{pmatrix} 1 \\ -0.3735 \\ -0.7309 \\ 0.5712 \end{pmatrix} \quad . \tag{3.2.13}$$

Using equation 3.2.10 the corresponding PC-pair to $\vec{S}_{\mathrm{corrected}}$ can be calculated to:

$$P_{\mathrm{corrected}} = 138.7^\circ \qquad C_{\mathrm{corrected}} = 31.3^\circ \quad . \tag{3.2.14}$$

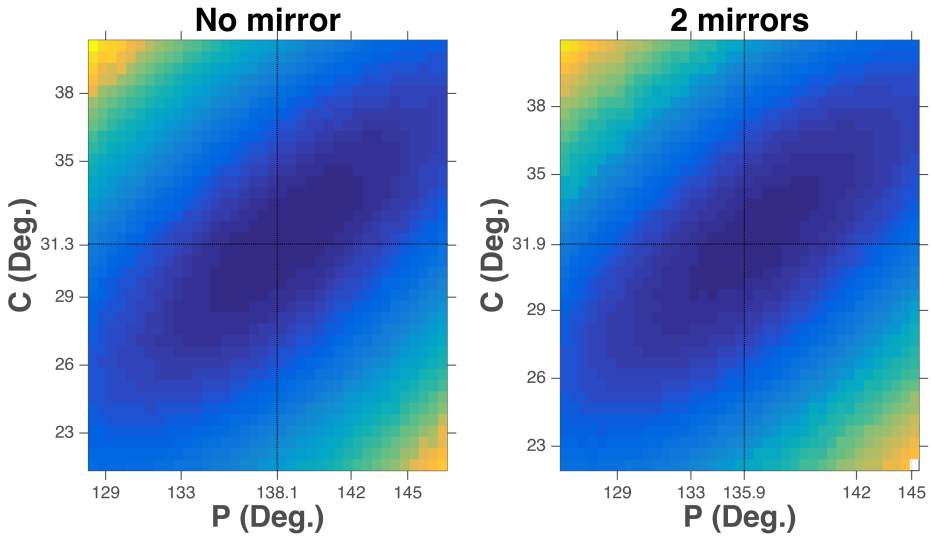

Figure 3.14 – Scanned PC-plane, left for a measurement no mirror, right a measurement taken with a combination of a m_2 followed by m_1. The minimum is found by taking the the point of lowest measured intensity. A more accurate value can be determined by fitting a paraboloid to the data, as presented in [Bau13]

The overlap between the three Stokes vectors is:

$$\arccos\left(\vec{S}'_{\text{nomirror}} \cdot \vec{S}'_{\text{mirror}}\right) = 0.0982 \tag{3.2.15}$$

$$\arccos\left(\vec{S}'_{\text{nomirror}} \cdot \vec{S}'_{\text{corrected}}\right) = 0.0133 \tag{3.2.16}$$

The improvement of overlap in equations 3.2.15 and 3.2.16 show, that for the measurements on a warm HOPG, the changes in the PC-plane could be explained by the polarization altering effects of the mirrors. With an analyser angle of 27.99° [Gre13] the complex refractive ratio can be calculated using equation 2.3.18:

no mirror	two mirrors	corrected
$\rho_s = 0.6373 - 0.4769i$	$\rho_s = 0.6901 - 0.4089i$	$0.6228 - 0.4876i$.

4 Summary and Outlook

As already shown in the dissertation of Beatrix Ostrick [Ost09] ellipsometry is a powerful tool, that is well suited for measuring the quality and thickness of films adsorbed on a HOPG. The new set up presented in Stephan Bauer's thesis [Bau13] shows that with modifications on the way the film is measured (changing from PA- to PC-ellipsometry) it is possible to monitor the film stability inside the new CKrS. The new CKrS, which is adapted to fulfil the requirements caused by the vertical set up inside the CPS, is still under construction and will be presented in an upcoming phd-thesis.
Since the new ellipsometry set up requires the use of mirrors, it was necessary to investigate the influence of said mirrors on ellipsometry measurements. Daniel Spitzer showed that ellipsometry via two 45° mirrors is possible. He did so by comparing the Krypton-reference-curves of measurements with and without mirrors. Because the new CKrS needs a different mirror set up, an attempt was made to characterize the mirrors used. Since the CKrS was not fully functional during this bachelor thesis a different approach, than the one presented in [Spi11], was chosen. Using the equipment given by ellipsometry set up, a RQP was build to measure the polarization state before and after each reflection. With the RQP it was possible to compare the polarization state before and after each reflection. The change in polarization was describable through a 3D rotation of the Stokes vectors. These rotations are presented as 4D Mueller matrix, allowing to calculate the polarization altering effects of the mirrors.
The method presented in this bachelors thesis has the advantage that it gives a quantitative understanding of the polarization change of the mirrors, as opposed to the phenomenological approach of comparing the krypton-reference-curves. The two measurements of section 3.2.2 on the warm HOPG showed that for this case the corrections in form of the determined Mueller matrices would improve the polarisation overlap by approximately one order of magnitude. Unfortunately, due to the not installed ablation laser, it was not possible to measure reference curves for the different set ups. Those measurements would be needed to show, that the loss of resolution explained in [Spi11]

could be explained by the polarization altering effects of the mirrors and not by other factors, like misalignment or unclean films. The calculated Mueller matrices show, that a beam reflected at the 15° mirror will represent a polarization state closer to the polarization state before reflection[1] than the 45° reflection angle mirrors. Even though both mirrors are from the same manufacturer and have the same coating material, they differ in quality. This difference probably comes from the fact, that for smaller angle of incidents the Fresnel coefficients for p- and s- polarized light are more similar than for angels close to the Brewster angle[2] (see figure 2.3).
Since ellipsometry via two 45° reflection angle mirrors was already successfully tested the combination of m_1 and m_2 should deliver even better results. If though the results would be unsatisfactory, the corrections shown in this thesis could be implemented into the ellipsometry evaluation routine presented in [Bau13], by correcting the PC-plane, or deriving a Jones matrix from the Mueller matrices presented and implementing it into the ellipsometry evaluation tools.

[1] Taking the phase shift for s-polarized light into account.
[2] Since it was not possible to find the refractive index of the coating material of the mirrors the it is guessed to be close to the refractive index of glass (1.5) the Brewster angle can be calculated by $\Theta_B = \arctan(1.5) \approx 56°$

Bibliography

[al.12] al., M. B.: Monitoring of the operation paramters of the KATRIN Windowless Gaseous Tritium Source. In: *New Journal of Physics* (2012), Nr. 14

[AP92] A. Picard, H. Barth et a. H. Backe B. H. Backe: A solenoid retarding spectrometer with high resolution and transmission for keV electrons. In: *Nuclear Instruments and Methods in Physics Research B* 63 (1992), Nr. 3

[Azz77] Azzam, Bashara (Hrsg.): *Ellipsometry and Polarized Light*. North Holland, 1977

[Bau13] Bauer, S.: *Energy calibration and stability monitoring of the KATRIN experiment*, Institut für Kernphysik der WWU, Diss., 2013

[BGS+13] Bauer, S. ; Grees, B. ; Spitzer, D. ; Beck, M. ; Bottesch, R. ; Ortjohann, H.W. ; Ostrick, B. ; Schäfer, T. ; Telle, H. H. ; Wegmann, A. ; Zboril, M. ; Weinheimer, C.: Ellipsometry with polarisation analysis at cryogenic temperatures inside a vacuum chamber. (2013)

[col04] collaboration, The K.: KATRIN Design Report. In: *FZKA Scientific Report* 38 (2004), Nr. 7090

[Flu08] Flueraru, Costel: Error Analysis of a Rotating Quarter-Wave Plate Stokes' Polarimeter. In: *IEEE TRANSACTIONS ON INSTRUMENTATION AND MEASUREMENT* 57 (2008), Nr. 4

[Gol10] Goldstein, D. H. (Hrsg.): *Polarized Light*. CRC Press, 2010

[Gre13] Grees, B.: *Verbesserung der Nullellipsometrie bei festem Analysatorwinkel für das KATRIN-Experiment*, Institut für Kernphysik der WWU, diploma thesis, 2013

[Jac02] Jackson, J. D. (Hrsg.): *Klassische Elektrodynamik*. De Gruyter, 2002

[KIT] *KIT Beta decay and MAC-E Filter*. `https://www.katrin.kit.edu/79.php`, . – Accessed: 2015-11-26

[Lob03] Lobashev, V. M.: The search for the neutrino mass by direct method in the tritium beta-decay and perspectives of study it in the project KATRIN. In: *Nuclear Physics A* 719 (2003), Nr. 1–4

[Mur02] Murayama, Hitoshi: The origin of the neutrino mass. In: *Physics World* (2002)

[Ost09] Ostrick, B.: *Eine kondensierte 83mKr Kalibrationsquelle für das KATRIN-Experiment*, Institut für Kernphysik der WWU, Diss., 2009

[Rob88] Robertson, D. A. K.: Direct Measurements of Neutrino Mass. In: *Annual Review of Nuclear and Particle Science* 38 (1988)

[Sal08] Saleh, Teich (Hrsg.): *Grundlagen der Photonik*. Wiley-VCH, 2008

[Sch11] Schaefer, T.: *Aufbau eines automatisierten Gassystems für die kondensierte 83mKr-Kalibrationsquelle des KATRIN-Experiments*, Institut für Kernphysik der WWU, diploma thesis, 2011

[Smo08] Smollich, J.: *Zählratenoprimierung und Hochspannungsmodifikation der kondensierten Konversionselektronen-Kryptonquelle (CKrS) für das KATRIN-Experiment*, Institut für Kernphysik der WWU, Diss., 2008

[Spi11] Spitzer, D.: *Alternative Ellipsomertie-Varianten bei kryogenen Temperaturen fuer das KATRIN-Experiment*, Institut für Kernphysik der WWU, diploma thesis, 2011

[Stu07] Sturm, M.: *Diplomathesis*, Institut für Kernphysik, Uni Karlsruhe, diploma thesis, 2007

[Thu07] Thuemmler, T.: *Präzisionsüberwachung und Kalibration der Hochspannung für das KATRIN-Experiment*, Institut für Kernphysik der WWU, Diss., 2007

[Val09] VALERIUS, K.: *Spectrometer-related background processes and their suppression in the KATRIN experiment*, Institut für Kernphysik der WWU, Diss., 2009

[Weg10] WEGMAN, A.: *Laserellipsometrie für die kondensierte Kr-Konversionselektronenquelle des KATRIN-Experiments*, Institut für Kernphysik der WWU, diploma thesis, 2010

I Appendix

I.1 RQP-measurements

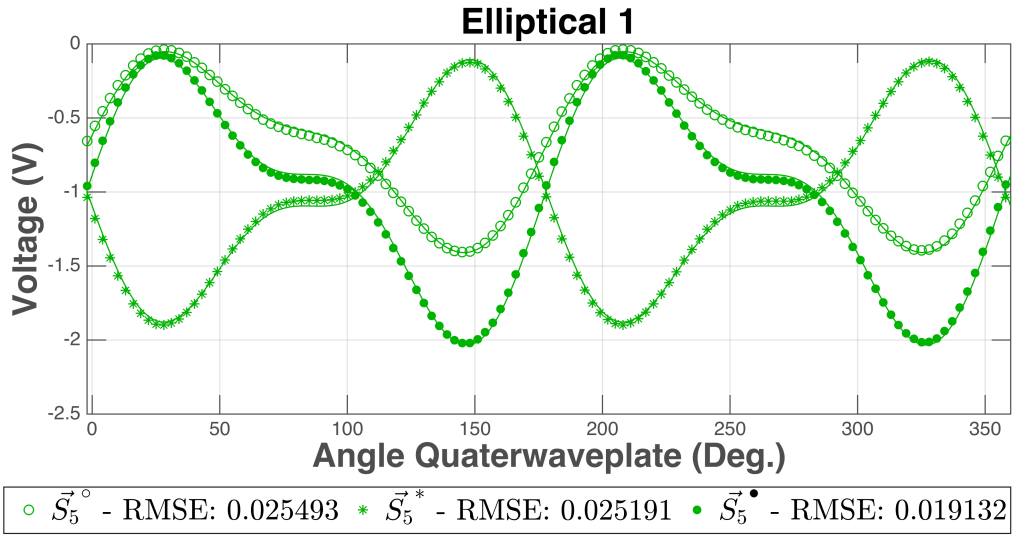

Figure I.1 – measurement 5, elliptically polarized.

Fitparameter figure I.1

$$\begin{pmatrix} -2.2436 \pm 0.0159 \\ 0.4713 \pm 0.0259 \\ 1.3968 \pm 0.0261 \\ -1.5132 \pm 0.0130 \end{pmatrix}^{\circ} \xrightarrow{15^{\circ}} \begin{pmatrix} -1.9156 \pm 0.0158 \\ -0.2754 \pm 0.0256 \\ -1.3475 \pm 0.0258 \\ 1.3637 \pm 0.0129 \end{pmatrix}^{*} \xrightarrow{45^{\circ}} \begin{pmatrix} -1.5197 \pm 0.0120 \\ 0.2871 \pm 0.0194 \\ 0.8345 \pm 0.0196 \\ -1.1316 \pm 0.0098 \end{pmatrix}^{\bullet}$$

Normed and corrected Stokes vectors for I.1

$$\begin{pmatrix} -0.9377 \pm 0.0285 \\ 0.0851 \pm 0.0137 \\ 0.7002 \pm 0.0212 \\ -0.7089 \pm 0.0196 \end{pmatrix}^{\circ} \xrightarrow{15^{\circ}} \begin{pmatrix} -1.1421 \pm 0.0212 \\ 0.0021 \pm 0.0136 \\ -0.7175 \pm 0.0192 \\ 0.6966 \pm 0.0154 \end{pmatrix}^{*} \xrightarrow{45^{\circ}} \begin{pmatrix} -0.9532 \pm 0.0240 \\ 0.0788 \pm 0.0143 \\ 0.6180 \pm 0.0185 \\ -0.7822 \pm 0.0181 \end{pmatrix}^{\bullet} \quad \text{(I.1.1)}$$

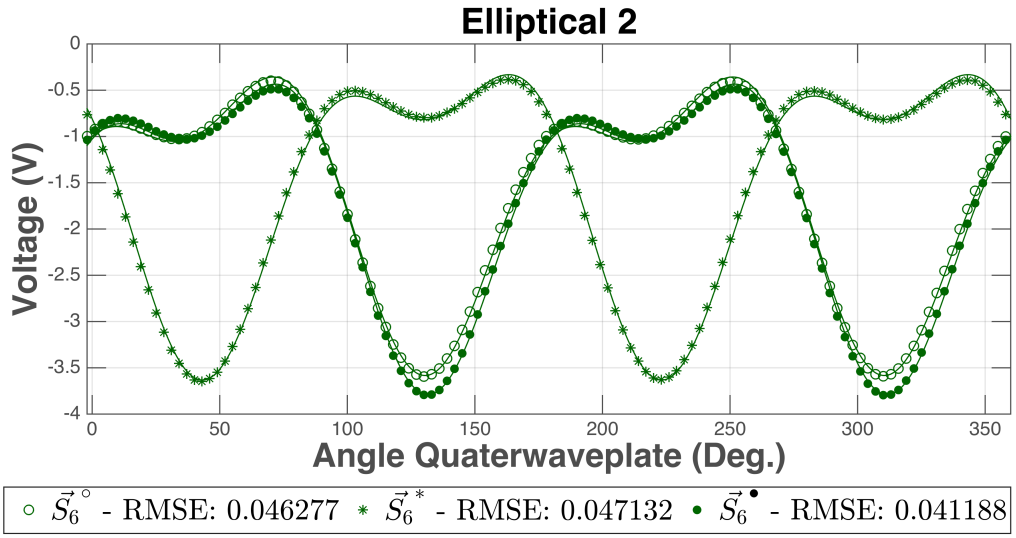

Figure I.2 – measurement 6, elliptically polarized.

Fitparameter figure I.2

$$\begin{pmatrix} -4.7255 \pm 0.0289 \\ 2.6700 \pm 0.0469 \\ -0.9800 \pm 0.0473 \\ -2.7955 \pm 0.0237 \end{pmatrix}^{\circ} \xrightarrow{15^{\circ}} \begin{pmatrix} -4.4181 \pm 0.0295 \\ 2.7979 \pm 0.0478 \\ -0.5355 \pm 0.0482 \\ 2.8303 \pm 0.0241 \end{pmatrix}^{*} \xrightarrow{45^{\circ}} \begin{pmatrix} -4.4466 \pm 0.0258 \\ 2.4474 \pm 0.0418 \\ -1.2335 \pm 0.0421 \\ -2.6219 \pm 0.0211 \end{pmatrix}^{\bullet}$$

Normed and corrected Stokes vectors for I.2

$$\begin{pmatrix} -1.2476 \pm 0.0602 \\ 0.7127 \pm 0.0358 \\ -0.1057 \pm 0.0172 \\ -0.6934 \pm 0.0359 \end{pmatrix}^{\circ} \xrightarrow{15^{\circ}} \begin{pmatrix} -1.1390 \pm 0.0561 \\ 0.7167 \pm 0.0372 \\ 0.0111 \pm 0.0139 \\ 0.6973 \pm 0.0362 \end{pmatrix}^{*} \xrightarrow{45^{\circ}} \begin{pmatrix} -1.2508 \pm 0.0581 \\ 0.7049 \pm 0.0336 \\ -0.1892 \pm 0.0195 \\ -0.6836 \pm 0.0345 \end{pmatrix}^{\bullet} \quad \text{(I.1.2)}$$

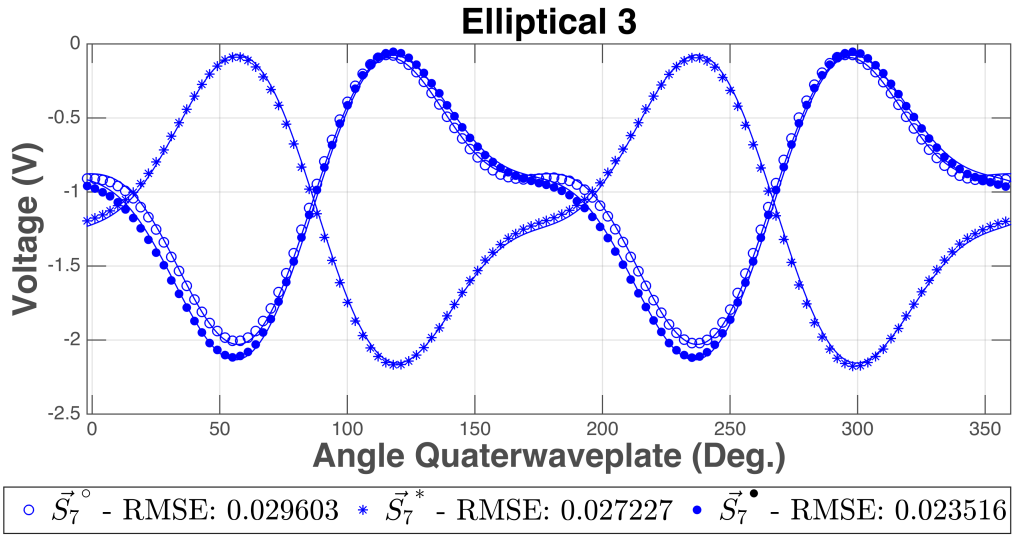

Figure I.3 – measurement 7, elliptically polarized.

Fitparameter figure I.3

$$\begin{pmatrix} -2.3066 \pm 0.0185 \\ 0.4496 \pm 0.0300 \\ 1.3357 \pm 0.0303 \\ 1.6819 \pm 0.0151 \end{pmatrix}^{\circ} \xrightarrow{15^{\circ}} \begin{pmatrix} -2.1732 \pm 0.0170 \\ -0.2664 \pm 0.0276 \\ -1.3531 \pm 0.0278 \\ -1.7145 \pm 0.0139 \end{pmatrix}^{*} \xrightarrow{45^{\circ}} \begin{pmatrix} -2.2451 \pm 0.0147 \\ 0.4916 \pm 0.0239 \\ 1.4582 \pm 0.0240 \\ 1.4812 \pm 0.0120 \end{pmatrix}^{\bullet}$$

Normed and corrected Stokes vectors for I.3

$$\begin{pmatrix} -0.9390 \pm 0.0302 \\ 0.0779 \pm 0.0150 \\ 0.6455 \pm 0.0218 \\ 0.7598 \pm 0.0223 \end{pmatrix}^{\circ} \xrightarrow{15^{\circ}} \begin{pmatrix} -1.1268 \pm 0.0213 \\ 0.0064 \pm 0.0129 \\ -0.6347 \pm 0.0178 \\ -0.7727 \pm 0.0169 \end{pmatrix}^{*} \xrightarrow{45^{\circ}} \begin{pmatrix} -0.9217 \pm 0.0268 \\ 0.0876 \pm 0.0126 \\ 0.7224 \pm 0.0203 \\ 0.6859 \pm 0.0180 \end{pmatrix}^{\bullet} \quad \text{(I.1.3)}$$

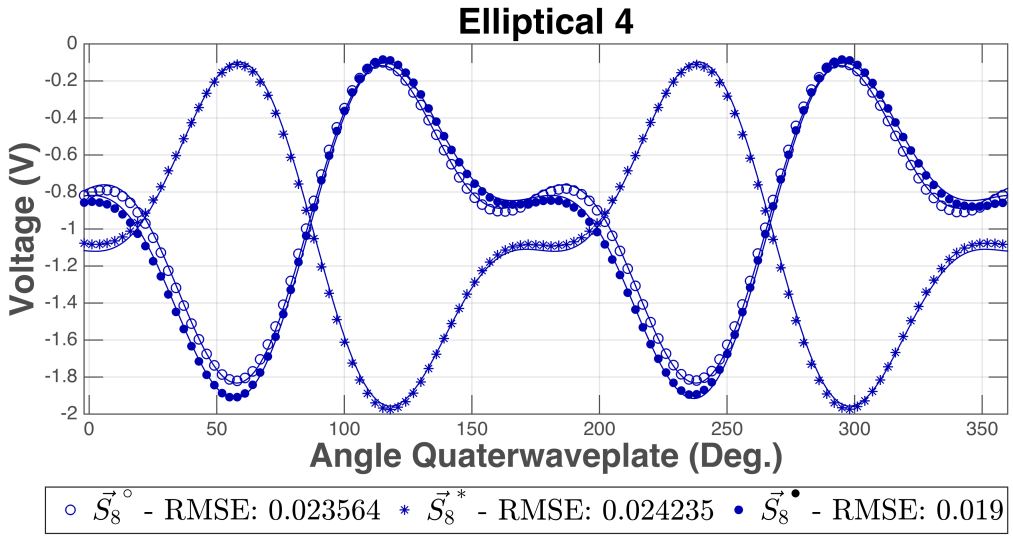

Figure I.4 – measurement 8, elliptically polarized.

Fitparameter figure I.4

$$\begin{pmatrix} -2.1532 \pm 0.0147 \\ 0.5159 \pm 0.0239 \\ 1.4015 \pm 0.0241 \\ 1.3610 \pm 0.0120 \end{pmatrix}^{\circ} \xrightarrow{15^{\circ}} \begin{pmatrix} -1.9907 \pm 0.0152 \\ -0.2475 \pm 0.0246 \\ -1.4649 \pm 0.0248 \\ -1.4074 \pm 0.0124 \end{pmatrix}^{*} \xrightarrow{45^{\circ}} \begin{pmatrix} -2.1125 \pm 0.0119 \\ 0.5523 \pm 0.0193 \\ 1.5138 \pm 0.0194 \\ 1.1815 \pm 0.0097 \end{pmatrix}^{\bullet}$$

Normed and corrected Stokes vectors for I.4

$$\begin{pmatrix} -0.9335 \pm 0.0296 \\ 0.1101 \pm 0.0138 \\ 0.7379 \pm 0.0222 \\ 0.6658 \pm 0.0191 \end{pmatrix}^{\circ} \xrightarrow{15^{\circ}} \begin{pmatrix} -1.1292 \pm 0.0219 \\ 0.0272 \pm 0.0124 \\ -0.7327 \pm 0.0195 \\ -0.6801 \pm 0.0158 \end{pmatrix}^{*} \xrightarrow{45^{\circ}} \begin{pmatrix} -0.9099 \pm 0.0261 \\ 0.1176 \pm 0.0118 \\ 0.8038 \pm 0.0207 \\ 0.5832 \pm 0.0150 \end{pmatrix}^{\bullet} \tag{I.1.4}$$

II Plagiatserklärung des Studierenden

Hiermit versichere ich, dass die vorliegende Arbeit mit dem titel "Adaption of the PC-Ellipsometry for the Condensed Krypton Calibration Source Setup, Converted for the Operation at the KATRIN-Experiment" selbstständig verfasst worden ist, dass keine anderen Quellen und Hilfsmittel als die angegebenen benutzt worden sind und dass die Stellen der Arbeit, die anderen Werken – auch elektronischen Medien – dem Wortlaut oder Sinn nach entnommenen wurden, auf jeden Fall unter Angabe der Quelle als Entlehnung kenntlich gemacht worden sind.

Münster, December 10, 2015

Ort, Datum Unterschrift

Ich erkläre mich mit einem Abgleich der Arbeit mit anderen Texten zwecks Auffindung von Übereinstimmungen sowie mit einer zu diesem Zweck vorzunehmenden Speicherung der Arbeit in eine Datenbank einverstanden.

Münster, December 10, 2015

Ort, Datum Unterschrift